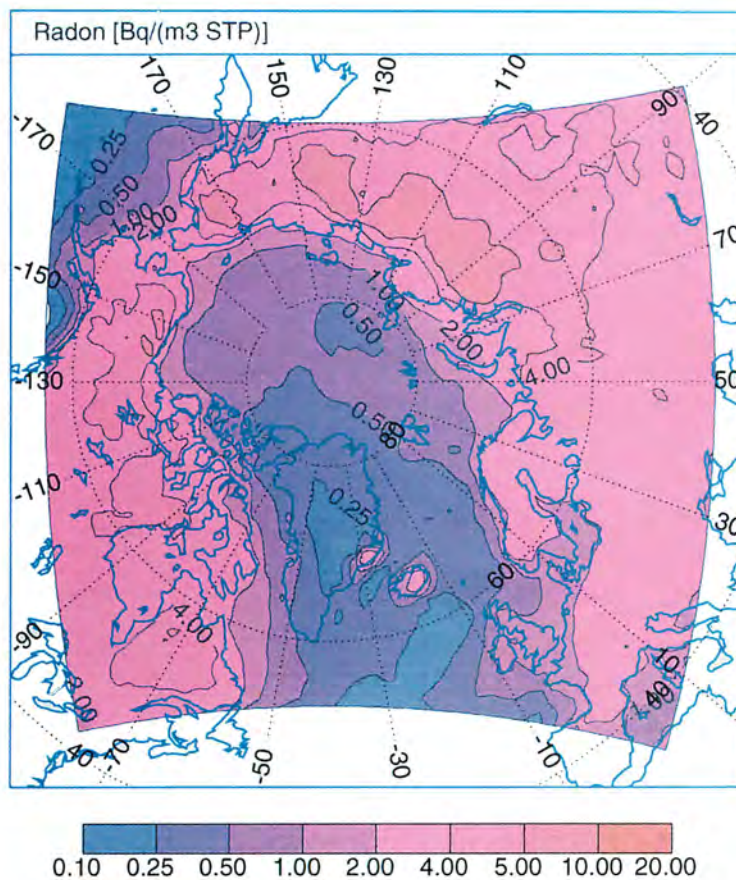


MATCH - Meso-scale Atmospheric Transport and Chemistry modelling system

Basic transport model description and control experiments with ^{222}Rn



Lennart Robertson and Joakim Langner
Swedish Meteorological and Hydrological Institute, SMHI

and

Magnus Engardt
Department of Meteorology, Stockholm University (MISU)

MATCH - Meso-scale Atmospheric Transport and Chemistry modelling system

Basic transport model description and control experiments with ^{222}Rn

Lennart Robertson and Joakim Langner
Swedish Meteorological and Hydrological Institute, SMHI

and

Magnus Engardt
Department of Meteorology, Stockholm University (MISU)

Report Summary / Rapportsammanfattning

Issuing Agency/Utgivare		Report number/Publikation	
Swedish Meteorological and Hydrological Institute S-601 76 NORRKÖPING Sweden		RMK No. 70	
		Report date/Utgivningsdatum	
		September 1996	
Author (s)/Författare			
Lennart Robertson and Joakim Langner, SMHI Magnus Engardt, MISU			
Title (and Subtitle/Titel)			
MATCH - Meso-scale Atmospheric Transport and Chemistry modelling system <i>Basic transport model description and control experiments with ²²²Rn</i>			
Abstract/Sammandrag			
<p>A limited area, off-line, Eulerian atmospheric transport model has been developed. The model is based on a terrain following vertical coordinate and a mass conserving, positive definite advection scheme, with small phase and amplitude errors. The objective has been to develop a flexible, all purpose off-line model. The model includes modules for emission input, vertical turbulent diffusion and deposition processes. The model can handle an arbitrary number of chemical components and provides a framework for inclusion of modules describing physical and chemical transformation processes between different components. Idealized test cases as well as simulation of the atmospheric distribution of ²²²Rn demonstrates the ability of the model to meet the requirements of mass conservation and positiveness and to produce realistic simulations of a simple atmospheric tracer.</p>			
Key words/sök-, nyckelord			
Eulerian, atmospheric transport, vertical diffusion, Radon-222, mass conservative transport			
Supplementary notes/Tilläg		Number of pages/Antal sidor	Language/Språk
		37	English
ISSN and title/ISSN och titel			
0347-2116 SMHI Reports Meteorology Climatology			
Report available from/Rapporten kan köpas från:			
SMHI S-601 76 NORRKÖPING Sweden			

MATCH - Meso-scale Atmospheric Transport and Chemistry modelling system

Basic transport model description and control experiments with ^{222}Rn

Lennart Robertson and Joakim Langner
Swedish Meteorological and Hydrological Institute (SMHI)

and

Magnuz Engardt
Department of Meteorology, Stockholm University (MISU)

Abstract. A limited area, off-line, Eulerian atmospheric transport model has been developed. The model is based on a terrain following vertical coordinate and a mass conserving, positive definite advection scheme, with small phase and amplitude errors. The objective has been to develop a flexible, all purpose off-line model. The model includes modules for emission input, vertical turbulent diffusion and deposition processes. The model can handle an arbitrary number of chemical components and provides a framework for inclusion of modules describing physical and chemical transformation processes between different components. Idealised test cases as well as simulations of the atmospheric distribution of ^{222}Rn demonstrates the ability of the model to meet the requirements of mass conservation and positiveness and to produce realistic simulations of a simple atmospheric tracer.

Key words: Eulerian, atmospheric transport, vertical diffusion, Radon-222, mass conservative transport.

1. Introduction

Understanding the distribution and fluxes of various atmospheric trace constituents requires a proper knowledge of atmospheric transport as well as of the relevant physical and chemical transformation and deposition processes for the trace species considered. Numerical modelling today presents a powerful way of analysing many problems related to atmospheric trace constituents. The increasing power of digital computers as well as a steady improvement in the quality and resolution of meteorological data has led to the development and successful application of three-dimensional atmospheric transport models on a range of scales from local to global. Representative examples of limited area transport models are e.g. the STEM model (Carmichel and Peters, 1984) and the RADM (Chang *et al.*, 1987) and EURAD (Ebel *et al.*, 1991) models. Over the last five years the Swedish Meteorological and Hydrological Institute (SMHI) has developed a limited area atmospheric transport model called MATCH (Meso-scale Atmospheric Transport and Chemistry modelling system). The work started with the development of a high resolution (5x5 km horizontal resolution) model for southern Sweden (Persson *et al.*, 1990). This model was built on a vertical structure with only three model layers: a surface layer with constant thickness, a second layer representing the atmospheric boundary layer, and a third reservoir layer. The height of the interface between layer two and three followed the spatial and temporal variation of the boundary layer height. This three-layer version of MATCH is used in air pollution applications over regions in Sweden up to the size of Sweden. See e.g. Persson *et al.* (1994), Langner *et al.* (1995), Langner *et al.* (1996). The need for a model that could be applied over a larger horizontal domain prompted the development of a model with more layers in the vertical. This multi-layer version of MATCH has now reached a stage in the development when it is used in many different applications, also outside SMHI. A proper documentation of the basic transport model is therefore called

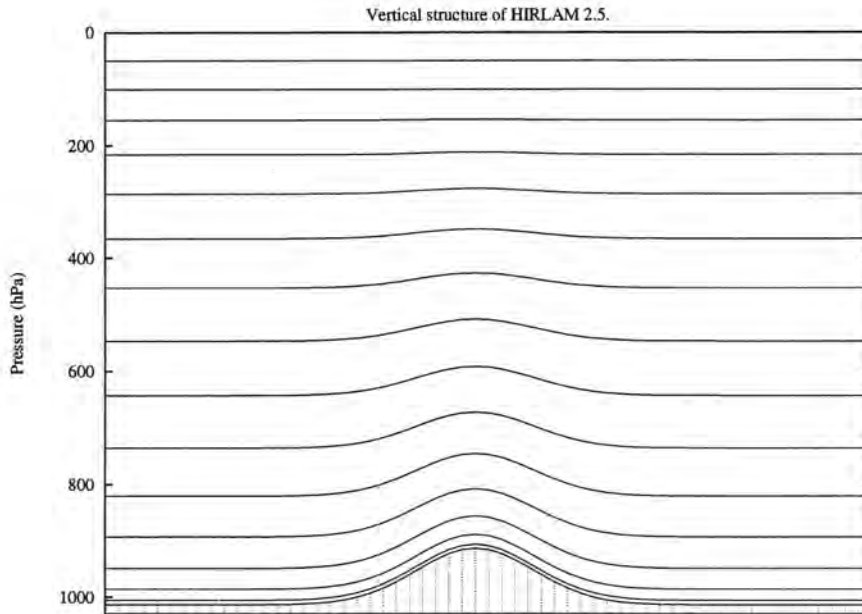


Fig. 1. Vertical structure of the MATCH transport model when HIRLAM 2.5 is used. Heights are given in pressure (hPa). The lowest contour assumes the ground surface, and the overlying atmosphere is divided into 16 layers.

for. This paper provides a description of the physical concepts on which the MATCH transport model is based and how these are implemented numerically. The results from a number of idealised test cases are presented along with simulations of the radioactive noble gas ^{222}Rn .

The MATCH model is described in section 2 followed by a discussion about balance between atmospheric mass and wind field (Section 3). Section 4 presents some tests of the numerical accuracy. A control experiment with ^{222}Rn is described in Section 5 and the paper is finalised with conclusions in Section 6.

2. Model description

2.1. MODEL STRUCTURE

The MATCH transport model is a three-dimensional “off-line” model, which means that atmospheric weather data are taken from some external source and fed into the model at regular time intervals, normally every 3 or 6 hours. Such data are usually interpolated in time to yield hourly data. Special attention is given to interpolation of the horizontal wind where vector increments are applied (see Appendix A). The vertical wind is calculated internally to assure mass-consistency of the atmospheric motion (see Section 3).

The trace species are represented as mass mixing ratios and prescribed boundary mixing ratios are treated in the same fashion as weather data, i.e read at regular time intervals and interpolated in time (see Section 2.7).

The model design is flexible with regard to the horizontal and vertical resolution, principally defined by the input weather data, and allows for an arbitrary number of chemical compounds. The model is written in η (or hybrid) vertical coordinates which is a linear combination of pressure, p , and σ vertical coordinates, where σ coordinates are defined as

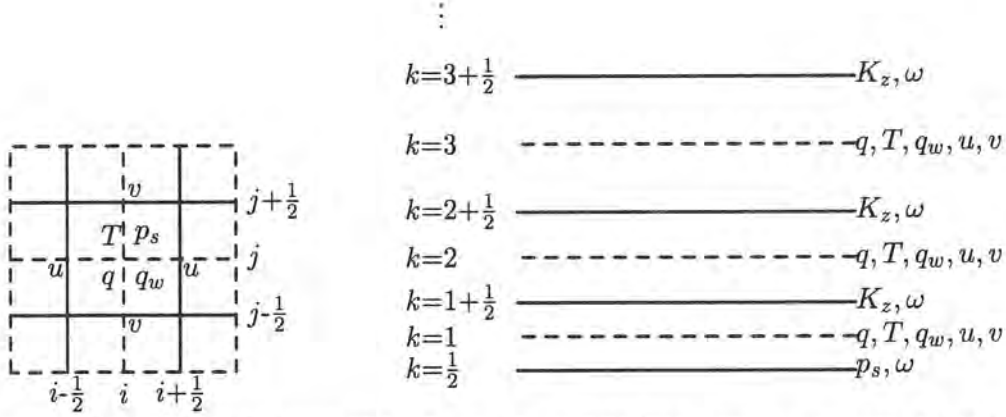


Fig. 2. Staggering of variables in the horizontal (left) and the vertical (right), where u, v, ω are the wind components, T is the temperature, q is the mixing ratio of the modeled component, q_w mixing ratio of water vapor, and K_z the exchange coefficient.

$$\sigma_i = \frac{p_i}{p_s}$$

where p_s is the surface pressure, and i refers to each vertical layer, thus

$$\eta_i = \frac{\alpha_i + \beta_i p_s}{p_s}$$

or

$$p_i = \eta_i p_s = \alpha_i + \beta_i p_s$$

Pressure and σ vertical coordinates can be obtained as special cases. Figure 1 shows the vertical resolution when HIRLAM 2.5 is used as input which is defined on hybrid coordinates (Källén, 1996). The horizontal wind components are staggered on an Arakawa-C grid, and the vertical wind and exchange coefficients are staggered in the vertical, see Figure 2.

2.2. TIME-SPLITTING

The physical processes that have to be considered for the fate of a trace-species in the atmosphere are injection pathways of anthropogenic and/or natural emissions into the atmosphere (A_Q), transport by the mean fluid motion ($A_u + A_v + A_\omega$) and turbulent eddies (A_T), transformation by chemical reactions (A_{CH}), and depletion by gravitational settling and by wet and dry deposition processes (A_D). The trace-species are considered non-buoyant (except during the very initial phase of release when buoyancy may be accounted for), and the input weather data are assumed to represent some time-scale longer than the lifetime of turbulent eddies, which then have to be treated in a parametric way. The time-split procedure outlined in Eqs. (1a,1b) is applied, where the mixing ratios, q , are updated for each process sequentially.

$$q^* = q^n + A_Q \quad (1a)$$

$$q^{n+1} = A_{CH}(A_u + A_v + A_w)A_D A_T q^* \quad (1b)$$

where A_Q is the emission vector, and A_T, A_D, \dots are the linear operators of the above mentioned processes. For non-linear chemistry is Eq. (1b) split into one linear and one non-linear part, but the general time-split principle is the same. The advection is split into one-dimensional advection processes for each direction. Note that the advective step is operating on the same mixing ratios for all directions. This procedure is chosen in order to be consistent with vertical wind calculation and will ensure the stability of the solution, e.g. a constant mixing ratio distribution should stay constant. We have not yet implemented alternating of the various operators, i.e. reversing the order every even time-step, which may improve the accuracy.

There are several time-steps involved in the data flow through the model. In the first place the large time-step over which new weather data (Δt_{met}) and boundary mixing ratios (Δt_{bound}) are read. Secondly the ‘‘interpolated’’ period (usually 1 hour), and thirdly the advective timestep (Δt_{adv}) and substepping over vertical diffusion (Δt_{vdiff}) and the chemical reaction scheme (Δt_{chem}). Figure 3 shows the various time-stepping as implemented in MATCH.

2.3. BASIC EQUATIONS

In an Eulerian frame-work the mass conservation for a given volume is determined by the integrated exchange with the surroundings across the volume boundary and the integrated contribution from the internal stationary sources and sinks. With pressure vertical coordinates this continuity equation is given by,

$$\frac{\partial}{\partial t} \int_{\Omega} q d\Omega = \oint_A (-\mathbf{v}_n q) dA + \int_{\Omega} s d\Omega \quad (2)$$

where Ω is the volume of the grid-cell, $d\Omega$ is $dx dy dp$, A is the grid-cell boundary, q the momentaneous mixing ratio of the compound, $\mathbf{v}_n = (u_n, v_n, \omega_n)$ the momentaneous fluid velocity, normal to the grid-cell boundary (defined positive when directed outward from the cell), and s the momentaneous sum of the internal sources and sinks. Splitting the variables into mean and turbulent parts, $q = \bar{q} + q'$, $\mathbf{v}_n = \bar{\mathbf{v}}_n + \mathbf{v}'_n$ and $s = \bar{s} + s'$, respectively, and applying Reynolds averaging procedure yields

$$\frac{\partial}{\partial t} \int_{\Omega} \bar{q} d\Omega = \oint_A (-\bar{\mathbf{v}}_n \bar{q} - \overline{\mathbf{v}'_n q'}) dA + \int_{\Omega} \bar{s} d\Omega \quad (3)$$

where $\overline{\mathbf{v}'_n q'}$ is the 3-dimensional turbulent flux intensity across the grid cell boundary. For a discrete grid cell volume, $\Delta x \Delta y \Delta p$, the continuity equation reads,

$$\frac{\partial}{\partial t} \bar{q} \Delta x \Delta y \Delta p = \oint_A (-\bar{\mathbf{v}}_n \bar{q} - \overline{\mathbf{v}'_n q'}) dA + \bar{s} \Delta x \Delta y \Delta p \quad (4)$$

or

$$\begin{aligned} (\bar{q}^{t+\Delta t} - \bar{q}^t) \Delta x \Delta y \Delta p = \\ \int_t^{t+\Delta t} \left[\oint_A \left(-\bar{\mathbf{v}}_n(\tau) \bar{q} - \overline{\mathbf{v}'_n(\tau) q'(\tau)} \right) dA + \bar{s}(\tau) \Delta x \Delta y \Delta p \right] d\tau \end{aligned} \quad (5)$$

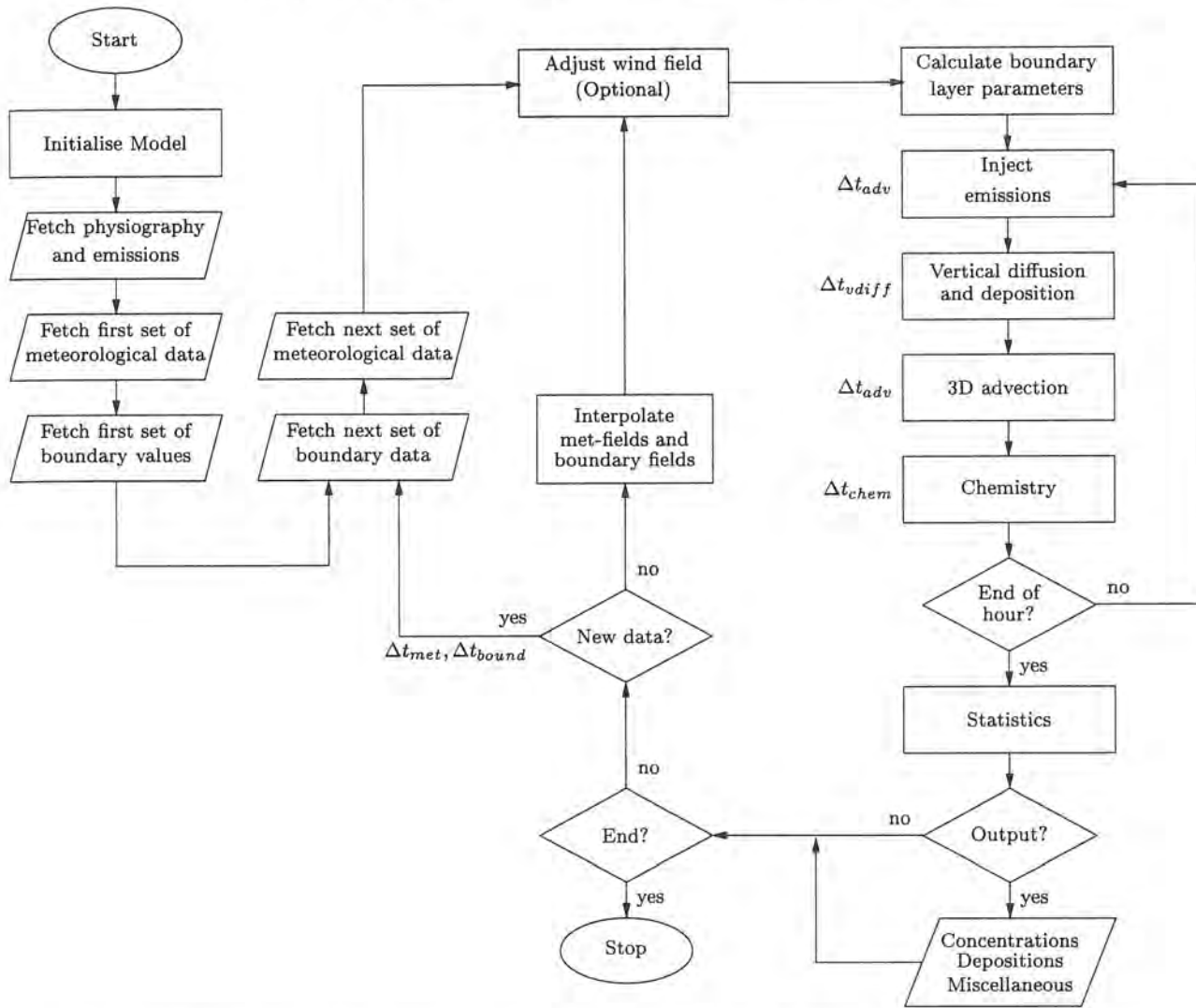


Fig. 3. Data flow and time-stepping in the MATCH model. Sub-stepping may take place for vertical diffusion (and deposition) and in the chemistry module, with time-steps Δt_{vdiff} and Δt_{chem} , respectively. Fetching new meteorology and boundary values may occur at different time intervals (Δt_{met} and Δt_{bound} , respectively).

where \bar{q} and \bar{s} represents the discrete grid cell average of mixing ratio and sources and sinks, respectively. The notation of mean and discrete values will be omitted hereafter.

2.4. ADVECTION

Numerical solution to the advection problem have been addressed by numerous authors, see e.g. Ostiguy and Laprise (1990), Dardub and Seinfeld (1994) for an overview. Williamson and Rash (1988), Williamson (1989) and Rash and Williamson (1990) pointed out the deficiencies of spectral methods applied to tracers with sharp gradients and suggested shape preserving and monotone interpolation schemes for semi-Lagrangian transport algorithms. Ritchie (1985) proposed a non-interpolation semi-Lagrangian scheme primarily for applications in dynamics. The semi-Lagrangian approach has suffered from poor mass conservation properties addressed by Leslie and Purser (1995). Their mass-conservative approach has similarities with the scheme suggested below in terms of the concept of primitive

functions. Bott (1989a, 1989b) further developed a family of one-dimensional positive definite and mass conservative Eulerian advection schemes suggested by Crowley (1968) and Tremback *et al.* (1987). Those schemes have been expanded fully into two dimensions by Rash (1993) and Hólmi (1994). The scheme implemented in MATCH is a generalisation of the class of mass conservative schemes suggested by Bott (1989a, 1989b) to arbitrary grid selections, by means of primitive functions described in Appendix B.

We apply the concept of operator-splitting into one-dimensional transport problems. For brevity only transport in one selected direction, the x-direction, is described hereafter. Following the notations by Bott (1989a) the continuity equation in one-dimension is given by,

$$q_i^{t+\Delta t} \Delta x \Delta y \Delta p = q_i^t \Delta x \Delta y \Delta p - [F_{x_i} - F_{x_{i-1}}] \quad (6)$$

where q_i is the discrete gridcell average value for the volume $\Delta x \Delta y \Delta p$, and F_{x_i} is the integrated advective flux across the cell interface at x_i according to Eq. (5),

$$F_{x_i} = \int_t^{t+\Delta t} \Delta y_{x_i} \Delta p_{x_i} u_{x_i}(\tau) q_{x_i}(\tau) d\tau \quad (7)$$

Here u_{x_i} and q_{x_i} are mean values over the cell interface $\Delta y_{x_i} \Delta p_{x_i}$. For a constant wind field the transport is equivalent to a rigid body motion, and the flux F_{x_i} across the cell wall at x_i equals the integrated mass along the upstream distance $\delta x = u \Delta t / \Delta x$ (Crowley, 1967). In a context of non-dimensional coordinates this yield,

$$F_{x_i} = \Delta y_{x_i} \Delta p_{x_i} \left[\Delta x_i \int_{\zeta_i - c^+}^{\zeta_i} q(\zeta) d\zeta - \Delta x_{i+1} \int_{\xi_i - c^-}^{\xi_i} q(\xi) d\xi \right] \quad (8)$$

where $\zeta = x / \Delta x_i$ and $\xi = x / \Delta x_{i+1}$ are non-dimensional coordinates, and c is the Courant number where $c^+ = 0.5(|u_{x_i}| + u_{x_i}) \Delta t / \Delta x_i$ and $c^- = 0.5(|u_{x_i}| - u_{x_i}) \Delta t / \Delta x_{i+1}$, respectively, positive or zero dependent on flow direction. Each of the integrals in (8) can be split in two parts as e.g.,

$$\int_{\zeta_j - c^+}^{\zeta_j} q(\zeta) d\zeta = \int_0^{\zeta_j} q(\zeta) d\zeta - \int_0^{\zeta_j - c^+} q^t(\zeta) d\zeta \quad (9)$$

thus the difference between two instances of the primitive function of q which are solved by Lagrange polynomial approximation from discrete integral values, described in Appendix B. For constant grid-spacing the above approach coincides with the area-preserving scheme (Bott, 1989b). The advantages of the proposed algorithm are three-fold. In the first place is the implementation of this algorithm trivial and secondly the algorithm is inherently applicable to non-uniform grid-spacing. Thirdly, the algorithm proves to be computationally more efficient (~ 10 % less floating point operations when comparing forth order polynomial schemes). Other aspects as monotonicity and non-oscillatory as addressed by e.g. Bott (1991) is not implemented so far.

This approach is applied in the horizontal with a fourth order polynomial scheme. In the vertical a zero order upstream scheme is applied. Flux limitation as proposed by Bott (1989a) is applied regarding all the fluxes in three-dimensions.

Flow dependent boundary conditions are applied. On the outflow boundary the gradient is prescribed (von Neuman condition) with assumed zero gradient in the mixing

ratio distribution over the boundary. On inflow a Dirichlet condition is applied with the prescribed boundary values assumed to be an infinite reservoir outside the domain.

2.5. BOUNDARY LAYER PARAMETERISATIONS

Boundary layer processes, such as stability dependent dry deposition flux and turbulent vertical mixing in the boundary layer, are parameterised by means of the three primary parameters, surface friction velocity (u_*), surface sensible heat flux (H_0) and the boundary layer height (z_{PBL}), from which some secondary parameters are derived as the convective velocity scale,

$$w_* = (gH_0/(\rho C_p T) z_{PBL})^{1/3} \quad (10)$$

and the Monin-Obukhov length,

$$L = \frac{u_*^3}{kgH_0/(\rho C_p T)} \quad (11)$$

where g is the acceleration of gravity, ρ is the air density, C_p is the specific heat of dry air at constant pressure, T is the temperature, and k is von Karmans constant.

2.5.1. Friction velocity

The friction velocity is derived for neutral stratification, in order to avoid unrealistic values of numerical origin for strongly stable or unstable conditions.

$$u_* = \frac{ku(z)}{\ln(z/z_0)} \quad (12)$$

2.5.2. Sensible heat flux

The sensible heat flux is given by the surface energy balance equation utilising formulations suggested by van Ulden and Holtslag (1985) for land areas and ice covered sea, and Burridge and Gadd (1977) for open sea areas.

The sensible heat flux for land and ice covered sea is defined from similarity theory by the surface friction velocity, u_* , and the temperature scale, θ_* ,

$$H_0 = -\rho C_p u_* \theta_* \quad (13)$$

van Ulden and Holtslag (1985) suggest different formulations of the temperature scale valid for daytime and nighttime boundary layer, respectively. Without going into any details the formulation for the daytime boundary layer reads,

$$\theta_* = -\frac{[(1-\alpha)S+1](1-C_g)Q_i^*}{(S+1)(1+C_h)\rho C_p u_*} + \alpha\theta_d \quad (14)$$

where α is a relative moisture parameter, S the slope of the saturation enthalpy curve, C_g the fraction of net radiation converted to ground heat flux, Q_i^* the isothermal net radiation, C_h an empirical heat coefficient and θ_d is an empirical temperature scale. The

net radiation is a function of the total cloudiness and the albedo as well as some other parameters. The albedo is determined by the surface and altered by presence of snow cover. For the nighttime boundary layer, θ_* is given by,

$$\theta_* = T_z \{ [(d_1 v_*^2 + d_2 v_*^3)^2 + d_3 v_*^2 + d_4 v_*^3]^{1/2} - d_1 v_*^1 - d_2 v_*^3 \} \quad (15)$$

where $v_* = u_*/(5gz)^{1/2}$, T_z is the temperature at first model level (at height $z = z_1$), and d_i are coefficients. For more details see van Ulden and Holtslag (1985). For open water a formulation suggested by Burridge and Gadd (1977) is used,

$$H_0 = C_H \Delta\theta \quad (16)$$

where $\Delta\theta = \theta_s - \theta_z$ is the potential temperature difference between the water surface and the first model level (at height $z = z_1$), and C_H is an exchange coefficient defined by,

$$C_H = \begin{cases} ku_*/\ln(z_1/z_0)(1 + 0.1\Delta\theta) & \text{for } \Delta\theta > -10 \\ 0 & \text{otherwise} \end{cases} \quad (17)$$

2.5.3. Boundary layer height

The boundary layer height is based on a bulk Richardson number approach (Holtslag *et al.*, 1995) for unstable conditions, $H_0 > 0$, where the boundary layer height is defined at the height where the bulk Richardson number, Ri , reaches a critical value, $Ri_{cr} = 0.25$. The bulk Richardson number at height z is defined as,

$$Ri_z = gz/\theta_1 \frac{\theta_z - \theta_s}{|\mathbf{v}_H|^2} \quad (18)$$

where

$$\theta_s = \theta_1 + 8.5 \frac{H_0}{\rho C_p w_m} \quad (19a)$$

$$w_m = (u_*^3 + 0.6w_*^3)^{1/3} \quad (19b)$$

where θ_1 is the potential temperature at the first model level, w_* the convective velocity scale (Holtslag *et al.*, 1995). For neutral and stable conditions, $H_0 \leq 0$, a recursive formulation proposed by Zilitinkevich and Mironov (1996) for the equilibrium stable boundary layer is used, that accounts for the combined effects of rotation, surface boundary flux and static stability in the free flow, and remains in force in the limits of rotation-free stable layer and perfect neutral layer subjected to rotation (Zilitinkevich and Mironov, 1996),

$$h^{n+1} = h^n - \frac{(a_1 h^n)^2 + a_2 h^n - 1}{2a_1^2 h^n + a_2} \quad (20)$$

$$(21)$$

where

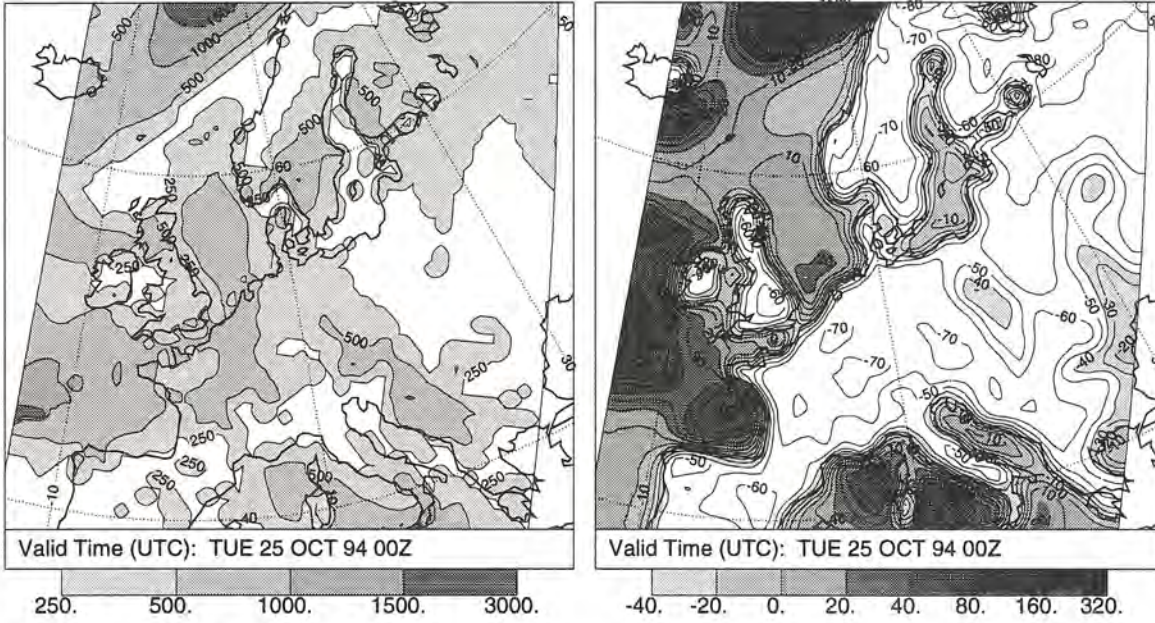


Fig. 4. An example of the atmospheric boundary layer height z_{PBL} (left, m) and surface sensible heat flux H_0 (right, $W m^{-2}$) derived in the MATCH model (see text).

$$a_1 = \frac{f}{C_n u_*} \quad (22a)$$

$$a_2 = \frac{1}{C_s L} + \frac{N_h}{C_i u_*} + \frac{|f|^{1/2}}{C_{sr} (u_* L)^{1/2}} + \frac{|N_h f|^{1/2}}{C_{ir} u_*} \quad (22b)$$

Here h converges to the equilibrium stable z_{PBL} , N_h is the Brunt-Väisälä frequency, f is the Coriolis parameter, and the coefficients $C_n = 0.5$, $C_s = 10$, $C_i = 20$, $C_{sr} = 1.0$ and $C_{ir} = 1.7$ (Zilitinkevich and Mironov, 1996). Figure 4 shows an example of boundary layer height and surface sensible heat flux as derived from the formulations above. Table I shows the input necessary to these schemes.

2.6. VERTICAL DIFFUSION AND DEPOSITION PROCESSES

The horizontal diffusive fluxes are assumed to be small compared to the advection along the direction of the horizontal wind. Only the vertical turbulent mixing is accounted for. Transport by deep convection is not considered so far. A first order approximation of the turbulent flux intensity from mixing length theory yields,

$$\overline{\omega'q'} = g\rho K_z \frac{\partial q}{\partial z} = -(g\rho)^2 K_z \frac{\partial q}{\partial p} \quad (23)$$

where K_z is the turbulent exchange coefficient yet to be determined. Mass conservation due to turbulent cross-boundary fluxes according to Eq. (5) then reads,

TABLE I
Input variables used for the surface energy balance scheme.

Temperature at lowest model level
Specific humidity at lowest model level
Wind at lowest model level
Surface temperature
Sea surface temperature
Ice coverage
Snow depth
Total cloud cover
Land use (water, forest, urban area , rural area)
Surface albedo
Surface roughness (z_0)

$$q_k^{t+\Delta t} \Delta x \Delta y \Delta p = q_k^t \Delta x \Delta y \Delta p + \Delta x \Delta y \int_t^{t+\Delta t} \left[(g\rho)^2 K_z \frac{\partial q(\tau)}{\partial p} \right]_{k+1/2} - \left[(g\rho)^2 K_z \frac{\partial q(\tau)}{\partial p} \right]_{k-1/2} d\tau \quad (24)$$

with the lower boundary condition

$$\left[(g\rho)^2 K_z \frac{\partial q(t)}{\partial p} \right]_{1/2} = g\rho v_d q(t) \quad (25)$$

where k is the vertical index of the grid-cell, and the indices $k + 1/2$ and $k - 1/2$ refer to the upper and lower grid-cell bounds in the vertical, respectively, and v_d is the dry deposition velocity. In the present implementation the lower boundary condition (25) is calculated explicitly before the vertical diffusion.

Over each time-step we assume the mean turbulent fluxes to be a weighted mean value of the fluxes at the bounds of the interval $[t, t + \Delta t]$, which lead us to a semi-implicit expression

$$q^{t+\Delta t} = q^t + \frac{\Delta t}{\Delta p} \left(\left[(g\rho)^2 K_z \left(\alpha \frac{\partial q^{t+1}}{\partial p} + \beta \frac{\partial q^t}{\partial p} \right) \right]_{k+1/2} - \left[(g\rho)^2 K_z \left(\alpha \frac{\partial q^{t+1}}{\partial p} + \beta \frac{\partial q^t}{\partial p} \right) \right]_{k-1/2} \right) \quad (26)$$

where $\alpha = 0.692$ and $\beta = 0.308$ (see Appendix C). Using a first order approximation of the mixing ratio gradient valid at the cell interfaces (see Eq. B.6), and the local density from the equation of state, we arrive at a final expression of the cross-boundary turbulent transport in terms of discrete grid-cell values

$$q_k^{t+1} = q_k^t$$

$$\begin{aligned}
& + \mathcal{K}_{k+1/2} \left(\alpha(q_{k+1}^{t+1} - q_k^{t+1}) + \beta(q_{k+1}^t - q_k^t) \right) \\
& - \mathcal{K}_{k-1/2} \left(\alpha(q_k^{t+1} - q_{k-1}^{t+1}) + \beta(q_k^t - q_{k-1}^t) \right)
\end{aligned} \quad (27)$$

where \mathcal{K} represents the non-dimensional turbulent Courant number, defined for the grid-cell from which the turbulent flux originate,

$$\mathcal{K}_{k+1/2} = \frac{(g\rho_{k+1/2})^2 2K_{z,k+1/2} \Delta t}{\Delta p_n (\Delta p_k + \Delta p_{k+1})} = \begin{cases} n = k & \text{for } q_{k+1} - q_k < 0 \\ n = k + 1 & \text{for } q_{k+1} - q_k > 0 \end{cases} \quad (28a)$$

$$\mathcal{K}_{k-1/2} = \frac{(g\rho_{k-1/2})^2 2K_{z,k-1/2} \Delta t}{\Delta p_n (\Delta p_k + \Delta p_{k-1})} = \begin{cases} n = k & \text{for } q_k - q_{k-1} > 0 \\ n = k - 1 & \text{for } q_k - q_{k-1} < 0 \end{cases} \quad (28b)$$

Eqs. (27,28a,28b) lead to a symmetric tri-diagonal system of equations, which is mass-conservative by the flux dependent definitions of the turbulent Courant number in (28a,28b).

Three different formulations of the exchange coefficient, K_z , are applied. The exchange coefficient within the boundary layer follows from suggestions by Holtslag *et al.* (1995) for neutral and stable conditions,

$$K_z(z) = \frac{ku_* z}{\phi_H(z, z_0, L)} (1 - z/z_{PBL})^2 \quad (29)$$

while the convective turn-over time z_{PBL}/w_* is utilised to directly determine the turbulent Courant number for the convective case,

$$\mathcal{K} = 1 - e^{-w_* \Delta t / z_{PBL}} \quad (30)$$

which asymptotically approach the case of rapid vertical mixing ($\mathcal{K} = 1$) with time-scales less than a time-step, Δt . The convective case is limited by $-z_{PBL}/L \geq 4$ or $w_*/u_* \leq 2.3$ (Holtslag *et al.*, 1995). Above the boundary layer, K_z , is defined explicitly from mixing length theory,

$$K_z = l^2 \frac{\partial |\mathbf{v}_H|}{\partial z} \quad (31)$$

where the mixing length, l , is kept constant. In the standard set up of MATCH l is set to zero. The stability function function ϕ_H is given by,

$$\phi_H(z, z_0, L) = \ln \left(\frac{z}{z_0} \right) - \psi_H \left(\frac{z}{L} \right) + \psi_H \left(\frac{z_0}{L} \right) \quad (32)$$

where ψ is based on the relationship proposed by Businger *et al.* (1971),

$$\psi_H(\xi) = \begin{cases} 2 \ln [(1+x)/2], & x = \sqrt{1-9\xi} \text{ for } \xi < 0 \\ -6.35\xi & \text{for } \xi > 0 \end{cases} \quad (33)$$

The dry deposition velocities found in the literature for different species are normally defined at a level of 1m. The lowest model level always represent a deeper layer and the deposition velocity has to refer such depth. Assuming constant dry deposition fluxes

through the lowest model layer yields an expression for a representative dry deposition velocity (Langner and Rodhe, 1991),

$$v_d = \frac{v_d(1m)}{1 + v_d(1m)\phi_H(z, 1m, L)/(ku_*)} \quad (34)$$

Wet deposition is described as a linear dependency of the precipitation intensity and treated implicitly,

$$q^{t+1} = q^t - \lambda P^t(\alpha q^{t+1} + \beta q^t)\Delta t \quad (35)$$

where λ is the scavenging coefficient ($s^{-1}\text{hour mm}^{-1}$) and P^t is the precipitation intensity (mm hour^{-1}), and α and β as above. Vertical transport by gravitational settling is treated by an upstream scheme with compound dependent sedimentation velocities.

2.7. EMISSION AND BOUNDARY CONDITIONS

The basic version of the MATCH transport model includes modules for inclusion of area emissions of the simulated species. Emissions can be introduced at any vertical height in the model and at different heights simultaneously.

Emissions are initially distributed in the vertical based on a Gaussian plume formulation (Berkowicz *et al.*, 1986), evaluated at a downwind distance of $x = u_h\Delta t$, where u_h is the windspeed at the effective plume height. If desired, standard plume-rise calculations (Berkowicz *et al.*, 1986) can be performed based on stack parameters (stack diameter, effluent temperature and volume flux) that are given as input to the model. It is also possible to specify temporal variation in the emissions over the diurnal time scale as well as variations between days. The emissions that enter the model calculations are updated every hour to account for temporal variations and the influence of stability on the plume-rise and initial spread calculations.

In some applications the possibility to specify mixing ratios on the boundaries of the model domain is required. Boundary conditions can be specified either as a constant value for each boundary (the four sides and the top of the modelling domain) or can be read from external files. In the case of using external files it is possible to update the boundary mixing ratios at any regular time interval, which then are linearly interpolated in time. This possibility is useful when performing one-way nesting between a large-scale, e.g. global model, and a high resolution MATCH model on a limited area.

3. Adjustment of unbalanced wind fields

Depending on the source of meteorological data the three-dimensional wind field may not be in exact balance with the mass field, i.e. the continuity equation for air may not be exactly fulfilled. There are several possible sources of such errors. In particular we note the following:

- Spatial interpolation errors
- Low accuracy of the stored meteorological data
- Time interpolation errors

Spatial interpolation errors arise when the data are transformed from one spatial representation to another before use. For example, this is the case when using data from global spectral models, e.g. the ECMWF model. Time interpolation errors is introduced when the meteorological data are interpolated in time from e.g. six to one hour in the off-line model. Depending on the particular application these errors may or may not be of significance. In applications for trace species with short residence times, typically days to weeks, direct output from NWP models is usually balanced enough to be used directly without modification in an off-line model. For tracers with longer residence times an adjustment of the wind fields are necessary. Otherwise numerical errors will tend to obscure significant parts of the solution. In order to maintain a flexible model an optional adjustment module has been built into the MATCH transport model (see Figure 3).

3.1. METHOD

The adjustment is coupled to the calculation of the vertical wind and is based on the method described by Heimann and Keeling (1989). The vertical wind is calculated according to the continuity equation in η -coordinates given by

$$\frac{\partial}{\partial \eta} \frac{\partial p}{\partial t} + \nabla \cdot (\mathbf{v}_H \frac{\partial p}{\partial \eta}) + \frac{\partial}{\partial \eta} (\dot{\eta} \frac{\partial p}{\partial \eta}) = 0 \quad (36)$$

By integrating the continuity equation using the boundary conditions $\dot{\eta}=0$ at $\eta=0$ and $\eta=1$, we obtain the equation for the surface pressure tendency

$$\frac{\partial p_s}{\partial t} = - \int_0^1 \nabla \cdot (\mathbf{v}_H \frac{\partial p}{\partial \eta}) d\eta \quad (37)$$

and the equation for $\dot{\eta}$

$$\dot{\eta} \frac{\partial p}{\partial \eta} = (1 - \frac{\partial p}{\partial p_s}) \frac{\partial p_s}{\partial t} + \int_{\eta}^1 \nabla \cdot (\mathbf{v}_H \frac{\partial p}{\partial \eta}) d\eta \quad (38)$$

where p_s is the surface pressure (Källén , 1996). Eq. (37) simply states that the rate of change of the surface pressure matches the vertically integrated air mass convergence. By first calculating the surface pressure tendency we can integrate Eq. (38) from the surface and upwards and obtain $\dot{\eta}$ for each level in the model. If no adjustment is desired the resulting vertical wind field is used directly, together with the surface pressure tendency derived from the surface pressure field assuming a linear variation of the surface pressure in time. If the wind field is not in balance the surface pressure tendency calculated using Eq. (37) will be much larger in absolute numbers than what is derived from the surface pressure field. A correction can then be derived as follows (Heimann and Keeling 1989). Denote by \mathbf{F} the vertically integrated mass flux field

$$\mathbf{F} = g^{-1} \int_0^1 \mathbf{v}_H \frac{\partial p}{\partial \eta} d\eta$$

and by M , the vertically integrated air mass per unit area

$$M = g^{-1} p_s$$

Eq. (37) is reexpressed as

$$\frac{\partial M}{\partial t} = -\nabla \cdot \mathbf{F} \quad (39)$$

We now set

$$\mathbf{F} = \mathbf{F}_{obs} + \mathbf{F}_{cor} \quad (40)$$

where \mathbf{F}_{obs} denotes the vertically integrated mass flux estimated from the input meteorological data and \mathbf{F}_{cor} denotes a correction to be found so that Eq. (39) is fulfilled. Inserting Eq. (40) into (39) we obtain an equation for \mathbf{F}_{cor}

$$\nabla \cdot \mathbf{F}_{cor} = -\nabla \cdot \mathbf{F}_{obs} - \frac{\partial M}{\partial t} \quad (41)$$

Clearly \mathbf{F}_{cor} should contain no rotational part, hence it may be expressed as the gradient of a scalar potential ψ

$$\mathbf{F}_{cor} = \nabla \psi \quad (42)$$

and Eq. (41) results in

$$\nabla^2 \psi = -\nabla \cdot \mathbf{F}_{obs} - \frac{\partial M}{\partial t} \quad (43)$$

This Poisson equation is solved on the limited area of interest where the right hand side is calculated from the input meteorological data and ψ is assumed to vanish at some distance outside the domain. The vertically integrated mass flux correction is then calculated from Eq. (42), which is distributed uniformly in the vertical. To get a good balance we have to iterate the method.

4. Simple test cases

The numerical properties of the transport model outlined in the preceding sections can be illustrated with a few simple test simulations. The following three types of tests will be discussed in the following:

- Transport of a passive tracer with constant initial distribution and constant boundary values;
- Transport of a passive tracer with zero initial distribution and constant upper boundary;
- Transport of a passive tracer from a point source.

4.1. CONSTANT INITIAL DISTRIBUTION AND CONSTANT BOUNDARIES

Note that the mixing ratio should be constant in this case. Figure 5 shows the result from a 48 hour simulation of a passive tracer over the period 94-10-23 12 UTC to 94-10-25 12 UTC. The model was initialised with a constant mixing ratio of 1000 ppt(m)

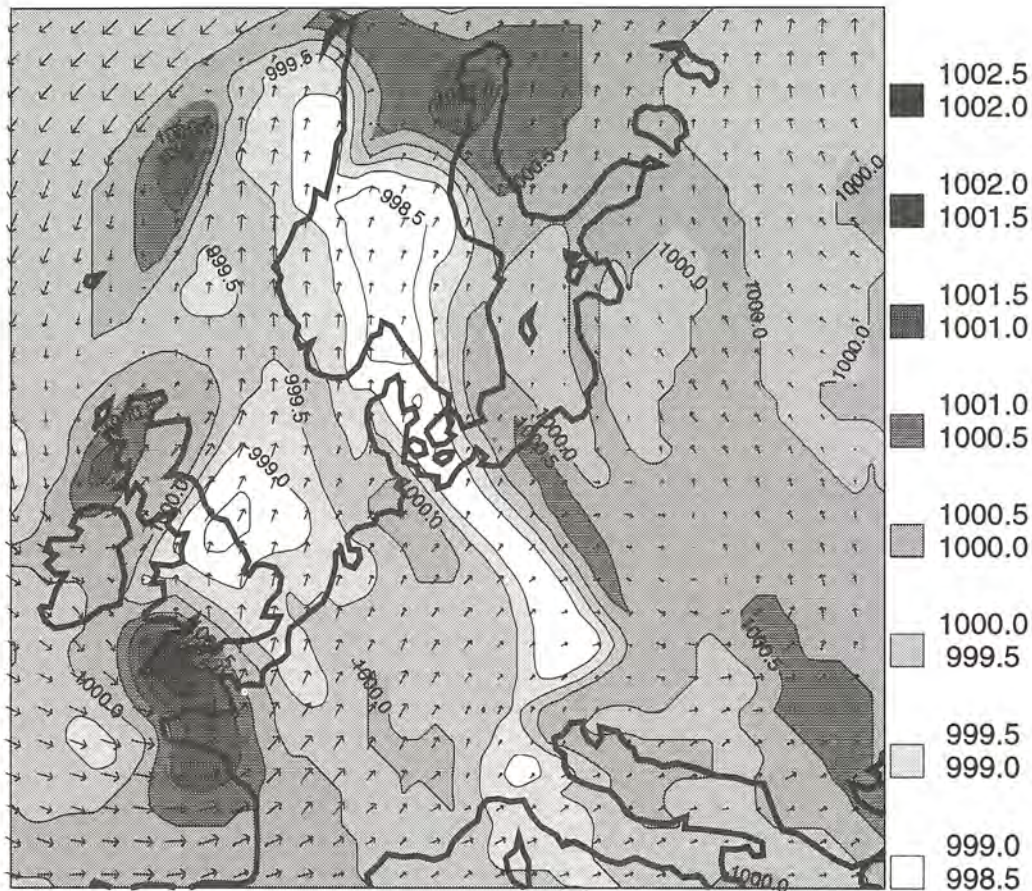


Fig. 5. Calculated distribution of a passive tracer after 48 hours of simulation starting from constant distribution of 1000 ppt(m) and with constant boundary values of 1000 ppt(m). The plot refers to layer 4, i.e. ~ 1 km above ground. The meteorological data is from 94-10-23 12UTC to 94-10-25 12 UTC. Units: ppt(m).

with the same value specified on all the model boundaries throughout the simulation. The meteorological data was taken from the operational HIRLAM 2.5 model at SMHI. The horizontal resolution is ca. 56 km with 16 levels in the vertical. Meteorological data was read every six hours and were then interpolated to one hour time resolution within MATCH, and the adjustment procedure outlined in Section 3 was used. The time-step was 300 s for advection and vertical diffusion. As can be seen the model is able to keep the mixing ratio constant to within about 2 permille. The plot shows the distribution at level four (~ 1 km) where the deviations are largest for this case. The budget calculations show that the mass is conserved to within five significant digits, using 32 bit arithmetics. These conservation properties are of major importance when simulating the distribution of long lived trace species like CO_2 where accuracy in simulated variations in the mixing ratio of less than one percent is required.

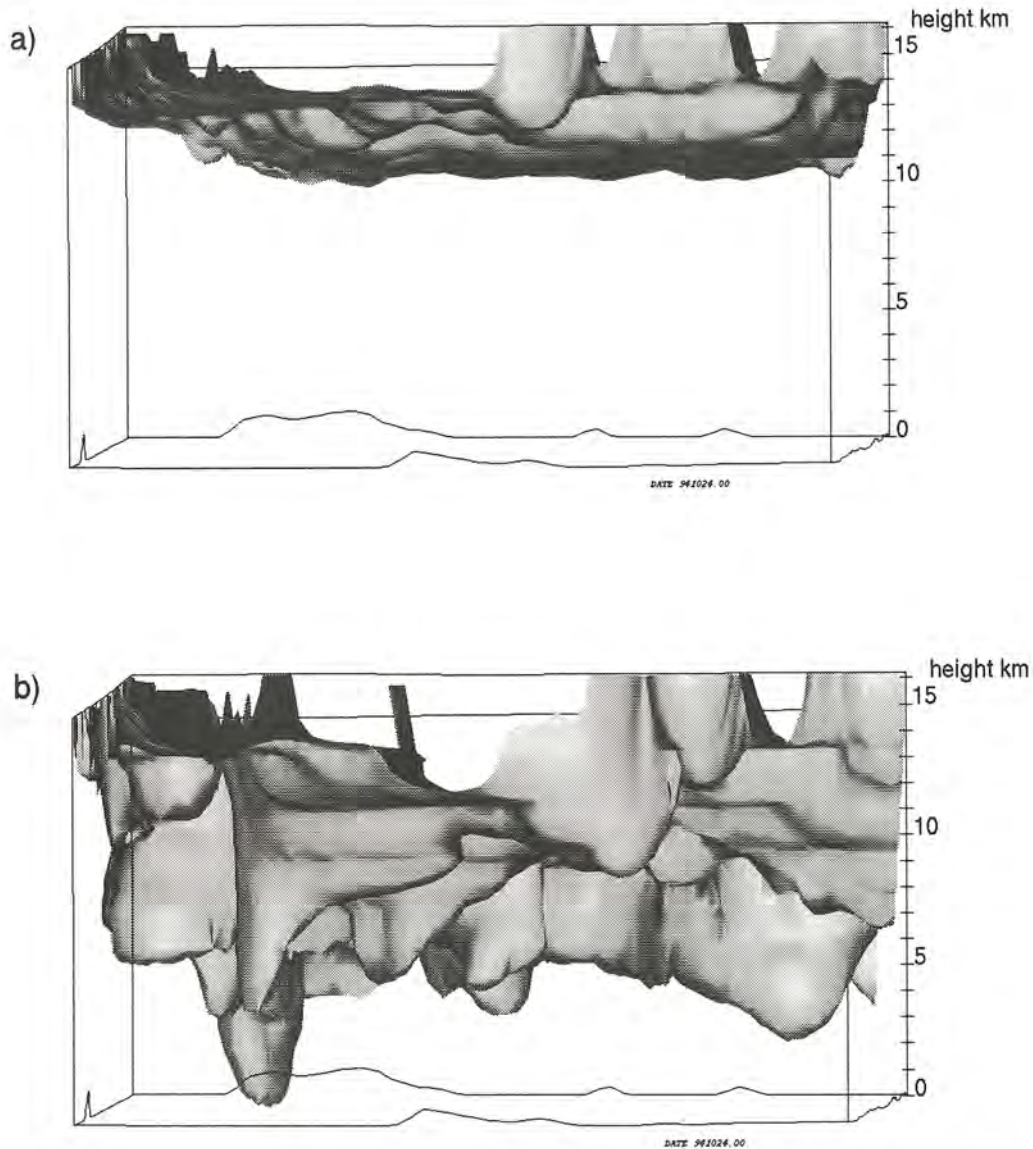


Fig. 6. Calculated penetration of a passive tracer from the top of the model domain, after 48 hours of simulation, starting from a zero initial distribution using data from HIRLAM, viewed from a location slightly below and to the left of the model domain. a) No adjustment, no time interpolation, b) No adjustment, time interpolation, c) With adjustment and time interpolation. Isosurface for 10 ppt(m). The mixing ratio at the upper boundary was fixed at 1000 ppt(m). Units: ppt(m).

4.2. ZERO INITIAL DISTRIBUTION AND CONSTANT UPPER BOUNDARY

The importance of the adjustment of the wind field described in section 3 are illustrated in Figures 6 - 7. Figure 6 shows the result from a 48 hour simulation of a passive tracer where the model was initialised with a zero mixing ratio. A mixing ratio of 1000 ppt(m) was specified at the top of the model and kept constant throughout the simulation. The meteorological data is the same as in the simulation described above. Figure 6a shows the

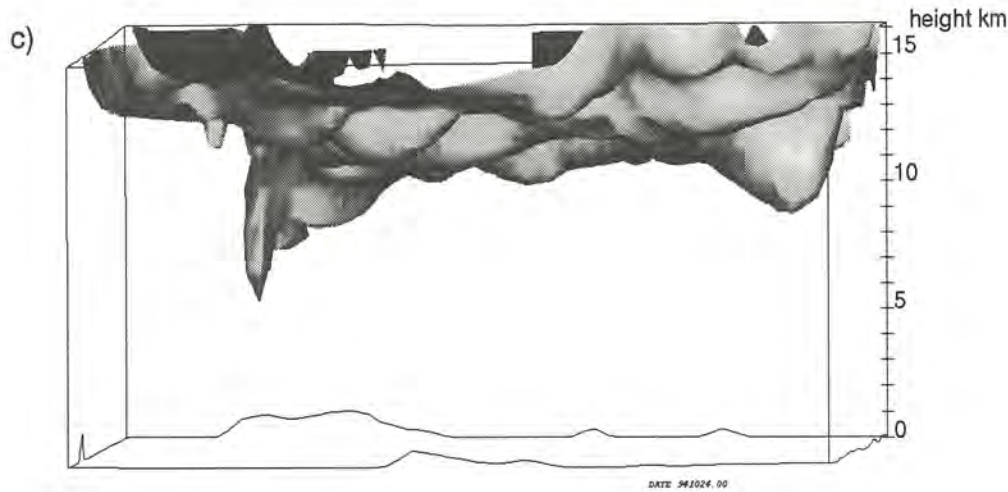


Fig. 6. Continued.

result when using unadjusted wind fields and no interpolation in time (i.e. the meteorological fields are kept constant for six hours between updates). The inflow is confined to the top layers reaching down to 11 km which appears quite realistic. Figure 6b shows a similar simulation but in this case the meteorological data from HIRLAM has been interpolated in time to one hour resolution within MATCH. No adjustment has been applied. Depending on location, the penetration of the inflow from the upper boundary varies. It reaches all the way down to about 1 km in one location connected to a trough region (cf. Fig 5). This is clearly unrealistic since the upper boundary is located well into the stratosphere. The corresponding results with adjusted wind fields are shown in Fig 6c. Here the penetration is much more limited and appears almost comparable to the case without time interpolation and without adjustment.

Figure 7 shows a similar simulation but now based on data from the ECMWF global model for the same period and geographical domain as above. The meteorological fields have in this case been interpolated from spectral space (T213) to a $0.5^\circ \times 0.5^\circ$ latitude longitude representation. The number of levels in the vertical is 31. Figure 7a shows the result when using unadjusted wind fields without time interpolation. The penetration is substantial reaching down to ca. 4.5 km which is clearly unrealistic. When time interpolation is introduced, Figure 7b, the result is even worse. As when using data from HIRLAM the penetration depends on location. Occasionally it reaches down almost to the surface. The corresponding results with adjusted wind fields are shown in Fig 7c. Here the penetration is much more limited, and also more limited than when using data from HIRLAM. The inflow is confined totally to the top four layers in the model which are all in the stratosphere. The difference compared to HIRLAM is probably due to higher vertical resolution which gives less numerical diffusion in the vertical advection, which is calculated using an upstream scheme, and a time-step of 300 s for both data sets. These simulations demonstrate the importance of ensuring that the wind field is in proper balance before use in an off-line transport model. The need for adjustment varies depending on the quality of the meteorological data. Using model output from HIRLAM without temporal inter-

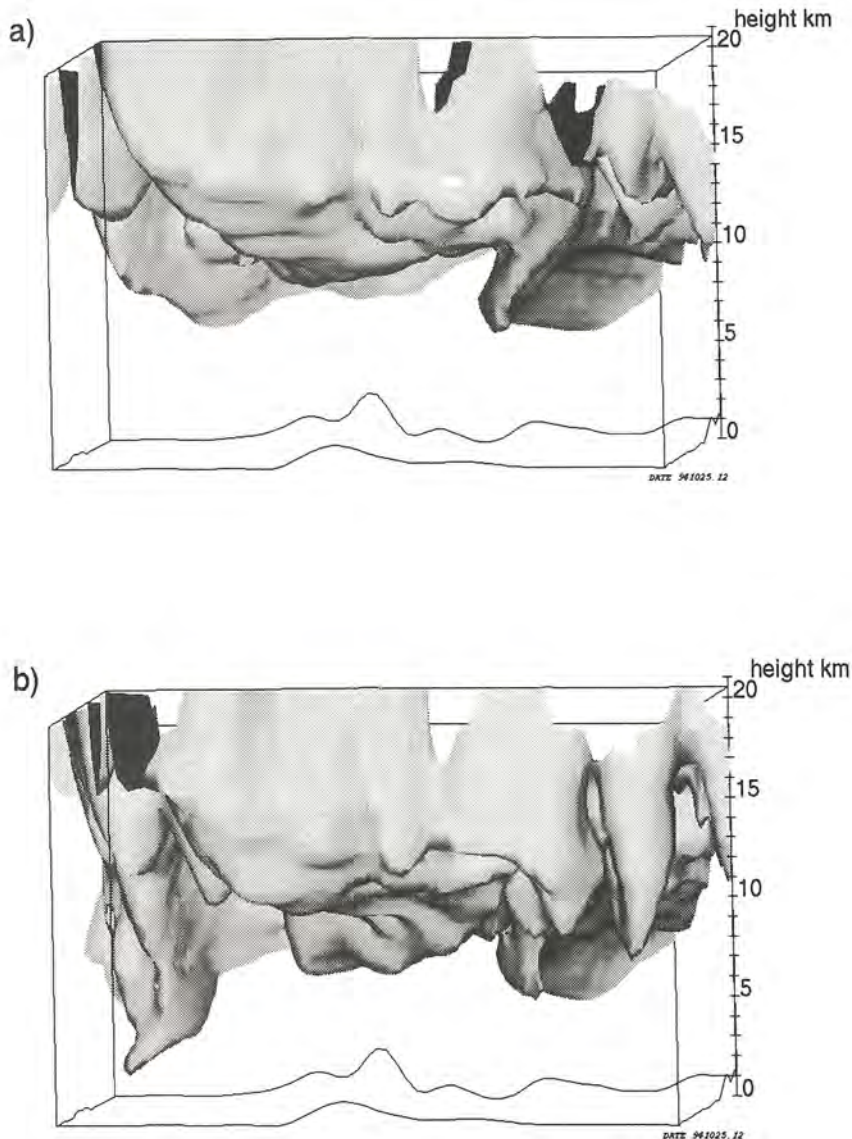


Fig. 7. Calculated penetration of a passive tracer from the top of the model domain, after 48 hours of simulation, starting from a zero initial distribution using data from ECMWF, viewed from a location slightly below and to the left of the model domain. a) No adjustment, no time interpolation, b) No adjustment, time interpolation, c) With adjustment and time interpolation. Isosurface for 10 ppt(m). The mixing ratio at the upper boundary was fixed at 1000 ppt(m). Units: ppt(m).

polation seems to give good results, indicating that the HIRLAM model output is well balanced. However, if time interpolation is used, the interpolated wind fields have to be adjusted. An alternative approach is of course to store data from the NWP model more frequently. The importance of the temporal resolution has been highlighted by Cats *et al.*

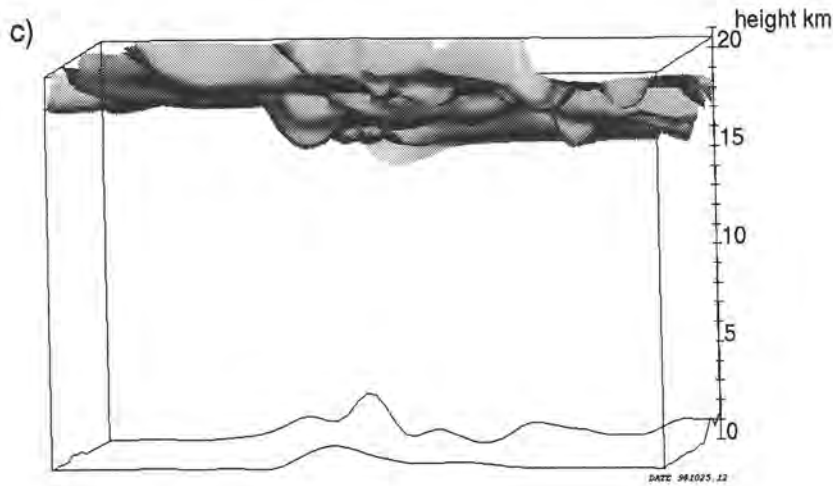


Fig. 7. Continued.

(1987) applying a trajectory model to the Chernobyl case with different update frequencies of input weather data. Cats *et al.* conclude that a time resolution of 1 hour is comparable with an “on-line” model. Horizontal interpolation also deteriorates the balance as in the ECMWF case. Before using meteorological data from a spectral model adjustment is clearly necessary.

4.3. SIMULATION OF RELEASE FROM A POINT SOURCE

As a final illustration of the performance of the model Figure 8 and 9 shows the evolution of a 12 hour release of a passive tracer from a surface point source located at 48°N , 2°W . Meteorological data are taken from HIRLAM and the period is the same as in the simulations discussed above. Figure 9 show the results when using the fourth order polynomial scheme in the horizontal advection. As can be seen the model is able to maintain sharp gradients in the distribution of the tracer. This is clearly in contrast to the results shown in Figure 10 where a zero order or upstream scheme has been used in the horizontal. In this case strong numerical diffusion is obvious and the distribution is very flat already 24 hours after the release. The mass is conserved in both simulations as well as the positiveness of the distribution. These simulations clearly demonstrates the importance of using higher order schemes for tracer advection.

It should be noted that proper handling of point sources demands an initialisation process to account for the sub-grid scale transport, during the initial phase of a point source release, before the cloud has reached a scale resolvable by the Eulerian model. The initialisation problem of point sources will be adressed in a later publication, and is not accounted for in this simulation. This means that the point source was momentarily spread over the whole grid-cell, where it is located, in the above simulations.

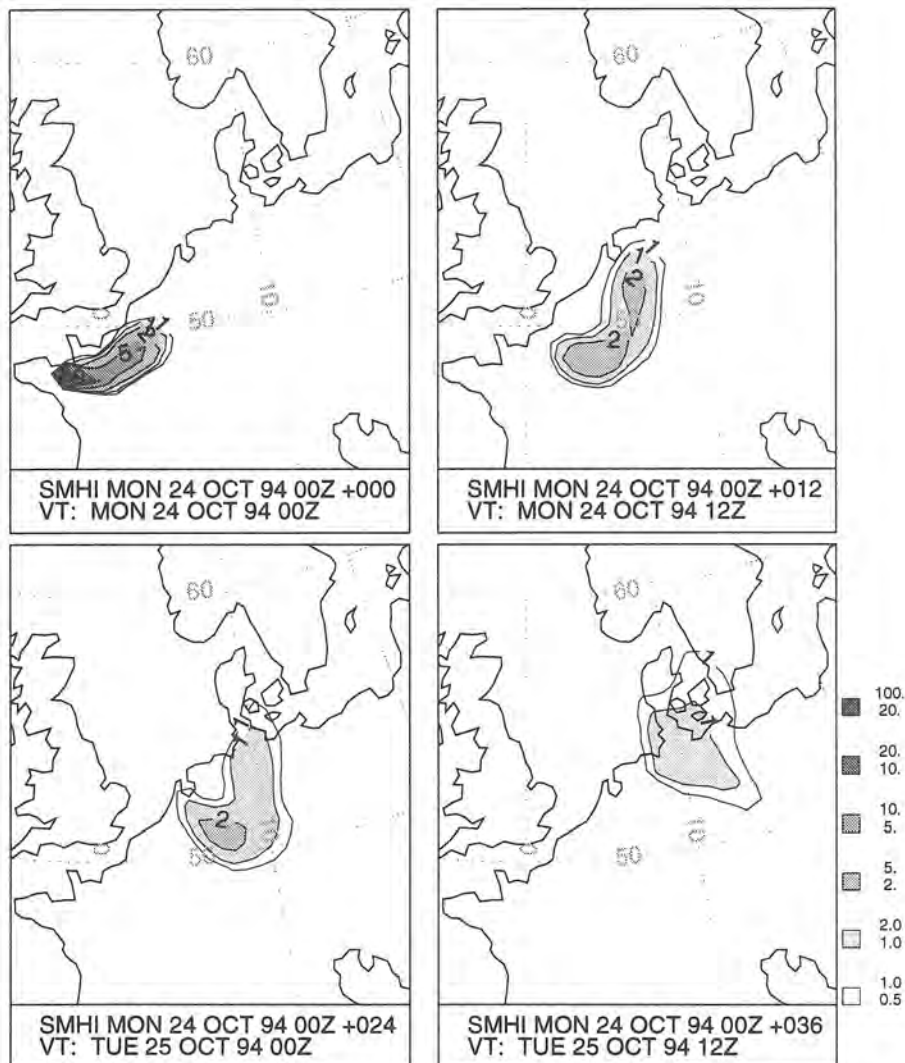


Fig. 8. Calculated distribution of a passive tracer released from a surface point source located at 48° N, 2° W using a fourth order scheme in the horizontal advection. The release starts at 94-10-23 12 UTC and stops 12 hours later. Resulting surface concentration after 12 (upper left), 24 (upper right), 36 (lower left) and 48 (lower right) hours of simulation. Arbitrary units.

5. Control experiment with ^{222}Rn

Radon is a noble gas with relatively low solubility in water (Schery *et al.*, 1984). The isotope with molar weight 222 (^{222}Rn) is an intermediate in the decay series of uranium-238 to lead-206. ^{222}Rn decays with a half-life of 3.8 days, by emitting an α -particle. It is emitted to the atmosphere from unglaciated surfaces of the earth, where it is produced through the decay of radium-226 (^{226}Ra , half-life 1.6×10^3 years). The flux from a given oceanic area is two orders of magnitude less than the corresponding terrestrial flux (Broecker *et al.*, 1967; Wilkening and Clements, 1975) and can be neglected, except possibly over remote areas of the oceans. The inertness to chemical reactions and cloud scavenging, the well defined source areas, and a radioactive lifetime similar to the meteorological time-scales, makes ^{222}Rn a suitable tracer to investigate horizontal and vertical transport in

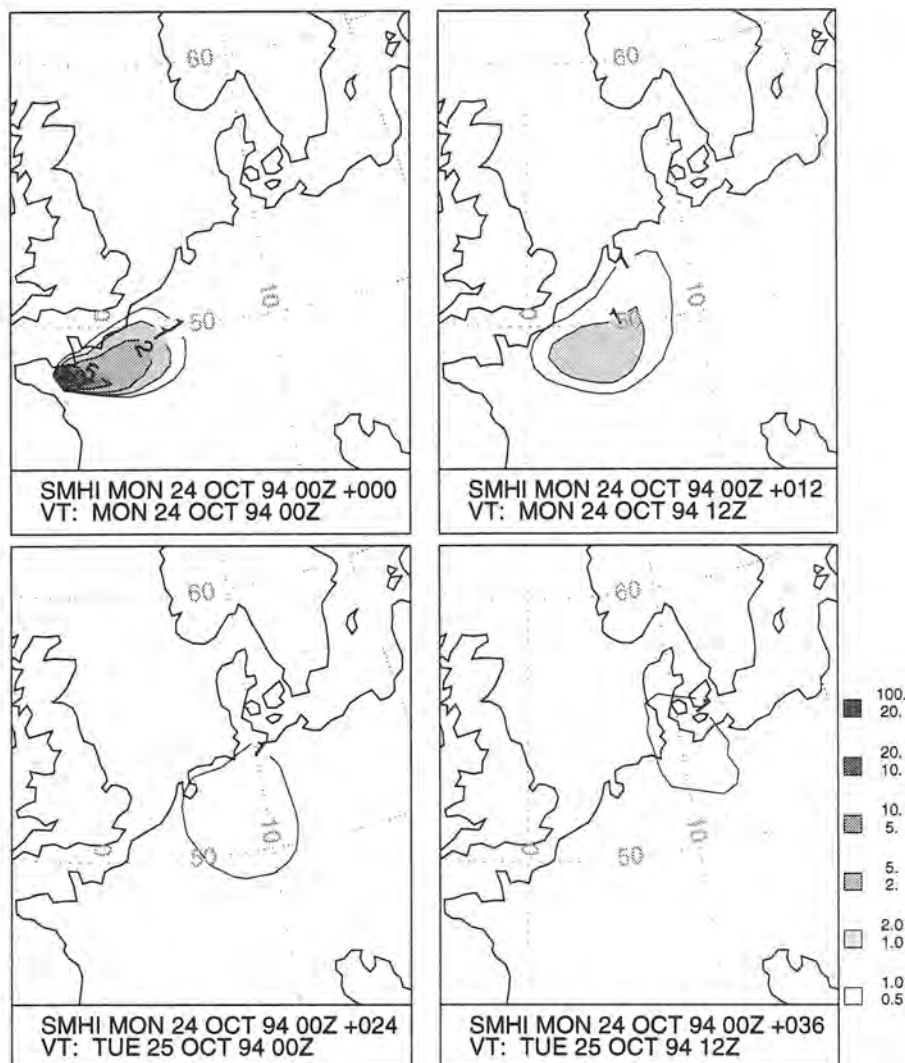


Fig. 9. Calculated distribution of a passive tracer released from a surface point source located at 48° N, 2° W using a zero order (upstream) scheme in the horizontal advection. The release starts at 94-10-23 12 UTC and stops 12 hours later. Resulting surface concentration after 12 (upper left), 24 (upper right), 36 (lower left) and 48 (lower right) hours of simulation. Arbitrary units.

the atmosphere. Measurements of ^{222}Rn are however scarce (especially vertical profiles), and displays large day-to-day variations due to changes in the local weather. There are also large spatial variations in the atmospheric concentration of ^{222}Rn , due to variations in the source function, which all complicates the interpretation of the data.

In order to validate a transport model and its parameterisations of the vertical flux, measured and simulated ^{222}Rn time-series and profiles should preferably coincide in time and space. This is especially true for MATCH, since it is driven by “real” meteorology and has a resolution which resolves the synoptic scale. Such data are, however, not available for the present study. After an initial discussion of the source function and a description of the experimental setup, we will in section 5.5, 5.6, and 5.7 compare our model results with other relevant measurements. In section 5.8 our results will be compared with published

studies with global three-dimensional transport models. Finally, section 5.9 will summarise the ^{222}Rn experiments.

The goal is not to present a refined distribution of ^{222}Rn in the troposphere, the results are presented to demonstrate the performance of MATCH during different seasons.

5.1. UNITS OF MEASURE

In MATCH, the concentration of a species is expressed in mass mixing ratios. Measurements of ^{222}Rn in the atmosphere are typically conducted by collecting the short-lived radon daughters (which quickly attach to particles) on filters and subsequently record the activity. The SI-unit for activity is 1 Bq ($= 1 \text{ s}^{-1}$), which, for some reason, is seldom used. Units in use are instead disintegration (or counts) per minute (1 dpm = 1 cpm = 1/60 Bq), or pCi (1 pCi = 1×10^{-12} Ci = 0.037 Bq). Furthermore, these units are most often normalised to standard temperature and pressure (STP) and hence directly proportional to our mass mixing ratios. We will hold on to SI-units and express all calculated ^{222}Rn mixing ratios in terms of activity at STP, and use the unit Bq m^{-3} (STP).

5.2. SOURCE TERM

The amount of ^{222}Rn emitted from a unit-surface of the Earth is highly variable, and contradictory estimates appear in the literature. The flux depends on a number of factors in the soil and on atmospheric conditions. The most important, apart from the ^{226}Ra content of the crustal material, are probably the soil porosity and possible inhibiting of the flux by overlying snow and ice. In a three year data-series from Chester (New Jersey, USA), reviewed by Jacob and Prather (1990), there is no correlation between ^{222}Rn flux and rainfall, while Mattsson (1970) interprets a minima in atmospheric ^{222}Rn concentrations in spring over several sites in Finland as due to an increased ground water table in the soil. Grasty (1992) reports large regional and inter-annual differences in atmospheric ^{222}Rn concentrations in summer-time for Canada, which were attributed to differences in precipitation.

Glaciers impede the flux from the underlying bedrock, as demonstrated by the very low ($\leq 0.04 \text{ Bq m}^{-3}$ (STP)) ^{222}Rn concentrations over Antarctica (Maenhaut *et al.*, 1979; Polian *et al.*, 1986). Jacob and Prather (1990) concluded from 129 flux measurements from Chester, that the ^{222}Rn flux was a factor 3 greater during non-freezing conditions than when the soil was frozen. These findings are also supported by other works cited in Feichter and Crutzen (1990). On the other hand, Larson (1974) argues against any inhibiting of the flux in winter, based on four profiles taken over Alaska in February, when the snow-cover was 0.6 m and high ^{222}Rn concentrations prevailed near the surface. Other, highly uncertain, factors affecting the magnitude of the flux include plowing and fertilising of cultivated land, ambient temperatures, local pressure changes and evapotranspiration from plants. Finally, the amount of ^{222}Rn reaching the free troposphere is obviously dependent on the atmospheric stability near the surface.

Due to the uncertainties in the quantification of the different factors affecting the terrestrial-atmospheric flux of ^{222}Rn we have in the following assigned all land surfaces south of 75°N a constant and uniform source of ^{222}Rn with the magnitude of $1.0 \text{ atoms cm}^{-2} \text{ s}^{-2}$. This appears to be in the middle of the range of the data in Table II. Grid-squares of Greenland and the Canadian Arctic, which has an elevation of more than 300 m above sea surface, are assumed to be glaciated and consequently have no ^{222}Rn flux to the atmosphere. Emissions from snow-covered land are not reduced, nor are the soil freezing or possible differences in soil moisture taken into account in the current study. The influence of varying soil content of ^{226}Ra is neglected since little information is available

TABLE II

Compilation of ^{222}Rn emission rates. Data are from both flux measurements and various model studies.

Emission from unglaciated land (atoms $\text{cm}^{-2} \text{s}^{-1}$)	Note	Reference
1.0 ⁽¹⁾	Source function in GISS 3D model; The flux is reduced by a factor of 3 under freezing conditions.	Balkanski <i>et al.</i> , 1993
1.2 ⁽¹⁾	Source function in MOGUNTIA; Flux reduced to 40% when snow-cover > 15 cm	Feichter and Crutzen 1990
0.72 ⁽¹⁾	Source function in ECHAM2; No reduction of flux during winter or heavy rains etc.	Feichter <i>et al.</i> , 1991
1.0 ⁽¹⁾	Source function in 2 GCMs (LMD & GISS); 1.0 atoms $\text{cm}^{-2} \text{s}^{-1}$ is ^{222}Rn production in soil. The flux to atmosphere is parameterised as a function of surface turbulence. Some of their experiments include an inhibiting of the flux when $T < 0 \text{ C}$.	Genthon and Armengaud, 1995
1.9 - 2.3	Measurements in N. America.	Graustein and Turekian, 1990
1.0 ⁽¹⁾	Source function in 3 global three-dimensional transport models (MOGUNTIA, TM1, AUTUMN). No reduction of flux during winter or heavy rains etc.	Heimann and Feichter, 1990
1.32 ⁽¹⁾	Estimated annual mean, global average, used as source in global 3D-model. No reduction of flux during winter or heavy rains etc.	Heimann and Keeling, 1989
1.0 ⁽¹⁾ , 0.33 ⁽¹⁾	The lower number is when 5-day mean temperature is below 0 C. Furthermore they use a correction factor for ^{222}Rn emancipation due to due to changes in surface pressure.	Jacob and Prather, 1990
0.72	Annual mean, global average.	Lambert <i>et al.</i> , 1982
1.05	From flux measurements in Australia	Schery <i>et al.</i> , 1989
1.2	Annual mean, global average.	Turekian <i>et al.</i> , 1977
0.7	Annual mean, global average	Wilkening <i>et al.</i> , 1972

⁽¹⁾ Estimates used as source function in transport models.

on this, and since this effect is believed to roughly cancel out when considering the size of the grid squares in this experiment. The effects of local stability is explicitly treated in MATCH through the temporal variation of the boundary layer parameters (see section 2.5 and 2.6).

5.3. NUMERICAL TREATMENT

The ^{222}Rn emissions are regarded as solely surface emissions with no buoyancy and introduced into the lowest model prior to the advection modules. The radioactive decay is calculated after the advection and is described by an explicit formulation,

$$q^{t+\Delta t} = q^t - \lambda q^t \Delta t$$

TABLE III
Predefined albedos for different surface types used to supplement the winter data set.

Surface type	Albedo
Sea	0.5
Land	0.15
Snow	0.8
Ice	0.75

where λ is the decay constant for ^{222}Rn ($2.097 \times 10^{-6} \text{s}^{-1}$), and $q^t, q^{t+\Delta t}$ are the old and new ^{222}Rn mixing ratios updated every time-step, Δt .

5.4. MODEL SETUP

The calculations below were performed using meteorological data from the T213 global weather prediction model of ECMWF. Initialised analyses with 6 hourly temporal resolution were interpolated to a rotated latitude-longitude grid with $1^\circ \times 1^\circ$ horizontal resolution. We used 30 unequally spaced layers in the vertical. The internal time-step was 300 seconds (for advection, vertical diffusion and radioactive decay, respectively), and the meteorological data were interpolated to 1 hour temporal resolution, with the adjustment procedure described in Section 3 applied. The model was initialised with zero ^{222}Rn mixing ratio and all boundaries set to zero throughout the integrations.

Two ECMWF data sets were utilised. The first one was from 15 May to 30 June 1994 representing spring and summer conditions. The second one was from 10 January to 28 February 1993 representing winter conditions. Cloud cover, snow depth and albedo which are used to calculate the boundary layer parameters, were not available in the second data set and had to be prescribed ad hoc. The total cloud cover was set to 4/8 over the entire area. Sensitivity tests with various cloud covers showed only marginally impact on the results, and we therefore regard the results to be uncorrupted by this crude treatment of the cloud cover. Snow cover was assigned to grid-cells where the temperature in the lowest model layer was below -5°C . The albedo was given by some predefined values for various surface types as shown in Table III. In the spring/summer experiment the boundary layer height was constrained to never exceed 2.5 km, in winter it was constrained to 1 km.

5.5. RESULTS: SPRING/SUMMER

While the ^{222}Rn activity in the model domain was zero at the beginning of the integration, an approximate steady state between the sources and sinks is reached within 10-15 days, see Figure 10.

Figure 11 shows the boundary layer height, z_{PBL} , and ^{222}Rn activity over 2 continental locations and one location in the Arctic. Over Central Europe (50°N , 10°E), the model calculates an atmospheric boundary layer that undergoes substantial diurnal variation. The ^{222}Rn activity near the surface is typically a factor of two higher during the morning hours compared to the local afternoon when the boundary layer depth is the greatest. The results are very similar to measurements in Germany during August and September (Dörr *et al.*, 1983) and in the eastern USA during summer (Jacob and Prather, 1990). At 1 km (layer 5), ^{222}Rn undergoes similar temporal variations as close to the surface, but the magnitude of the activity is lower.

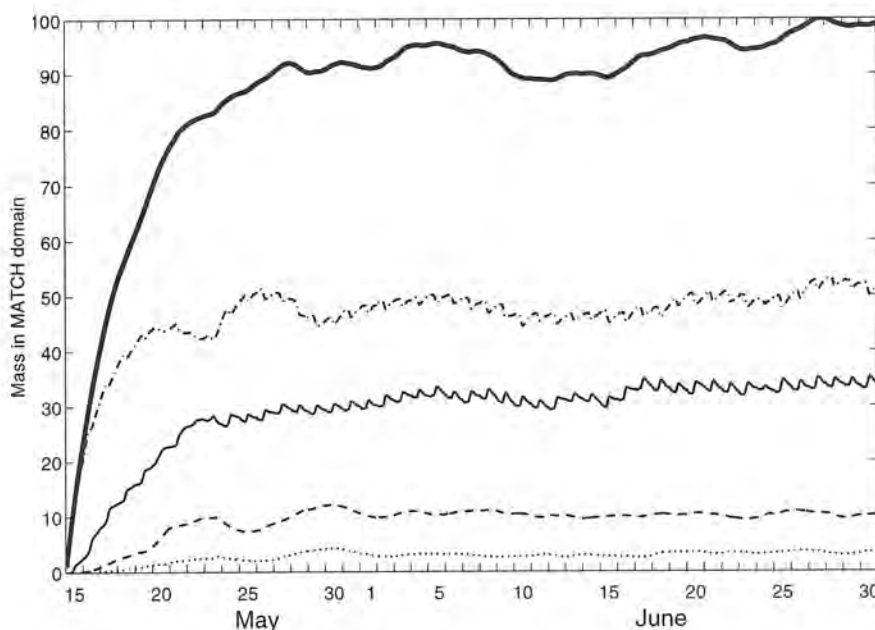


Fig. 10. Mass in model layers vs. integration time. The mass is normalised against maximum mass in all layers (representing 100 units). Thick solid line is total mass in MATCH domain; dash-dotted line is mass in layer 1-5; thin solid line is layer 6-10; dashed line is layer 11-15; dotted line is layer 16-30.

Northern Siberia (70°N , 110°E), is probably still snow-covered and the atmospheric boundary layer is dominantly stratified and thus more shallow. The diurnal temperature variation is also smaller and hence there is less prominent diurnal variation of ^{222}Rn near the surface. Day-to-day variations in boundary layer height are however seen and a shallow boundary layer during several days results in higher ^{222}Rn near the surface, whereas a deep boundary layer results in lower ^{222}Rn near the surface. On occasions the simulations show more ^{222}Rn in layer 5 than near the surface. This is most likely due to a combination of the efficient vertical mixing near the surface and upper air transport from other regions, enriched in ^{222}Rn .

Over an Arctic station (82°N , 62°W), the ^{222}Rn activity in layer 1 and 5 are most often similar. The peaks in ^{222}Rn are connected to long range transport from the source regions in Eurasia. Assuming a mean ^{222}Rn activity of 5 Bq m^{-3} in layer 1-5 over Northern Siberia (see Figure 12a), the peaks corresponds to a transit time of 5-10 days. There is no diurnal variation in the boundary layer height in the Arctic, and the calculated height is most often below 0.5 km with occasionally higher values. Since we have not specified any ^{222}Rn emissions near this site, changes in the local boundary layer is not affecting the ^{222}Rn activity.

Figure 12 shows average ^{222}Rn for June 1994 in model-layer 1 (0-60 m) and 15 (ca. 6 km above surface). The simulated ^{222}Rn in the lowest model layer is typically $4\text{--}5\text{ Bq m}^{-3}$ (STP) over the continents, maximum mean values occur in Northeastern Siberia and reaches 7 Bq m^{-3} (STP). Over the Arctic and the oceanic regions ^{222}Rn is below 1 Bq m^{-3} (STP). Lambert *et al.* (1982) estimates the annual mean ^{222}Rn activity to be 4.6 Bq m^{-3} (STP) over the northern hemisphere (NH) continents and 0.2 Bq m^{-3} (STP) over the NH oceans. Larson *et al.* (1972) report values around 0.1 Bq m^{-3} (STP) from ship measurements in the Greenland and Norwegian Sea during August. Leck *et al.* (1996) measured ^{222}Rn in the ice-covered Arctic and in the Fram strait in August and September,

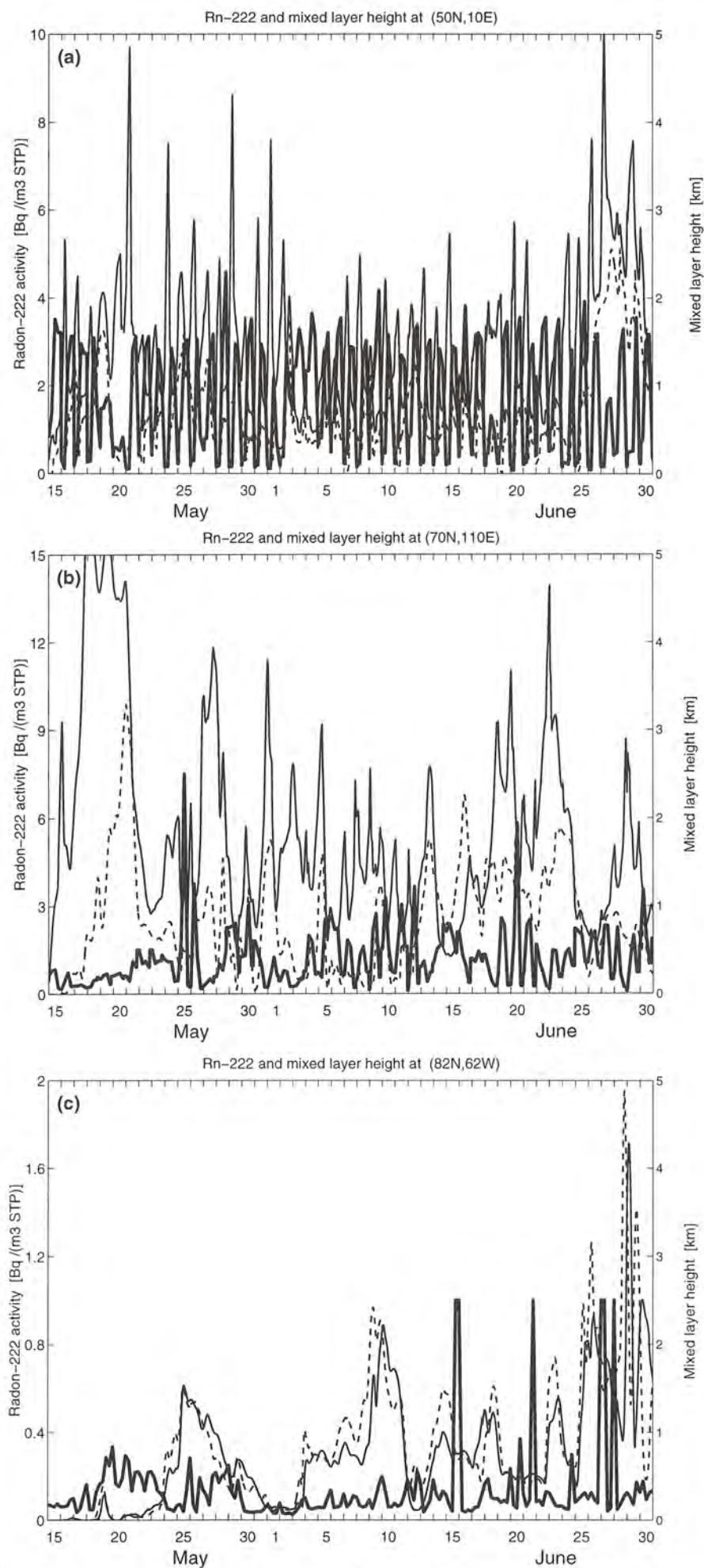


Fig. 11. Calculated boundary layer height, z_{PBL} , and ^{222}Rn activity for a summer period and 3 locations. a) Central Europe (50°N , 10°E), b) Northern Siberia (70°N , 110°E) and c) Canadian Arctic (82°N , 62°W). Thick solid line is boundary layer depth in km; thin solid line is the instantaneous ^{222}Rn activity every 1 hour at the lowest model layer and the dashed line is the corresponding ^{222}Rn activity at model layer 5. Note the different scales in the 3 panels.

their data range from $0.01 - 0.6 \text{ Bq m}^{-3}$ (STP). At model-layer 15 large regions have ^{222}Rn in excess of 0.1 Bq m^{-3} (STP), and maximum values reach 0.4 Bq m^{-3} (STP).

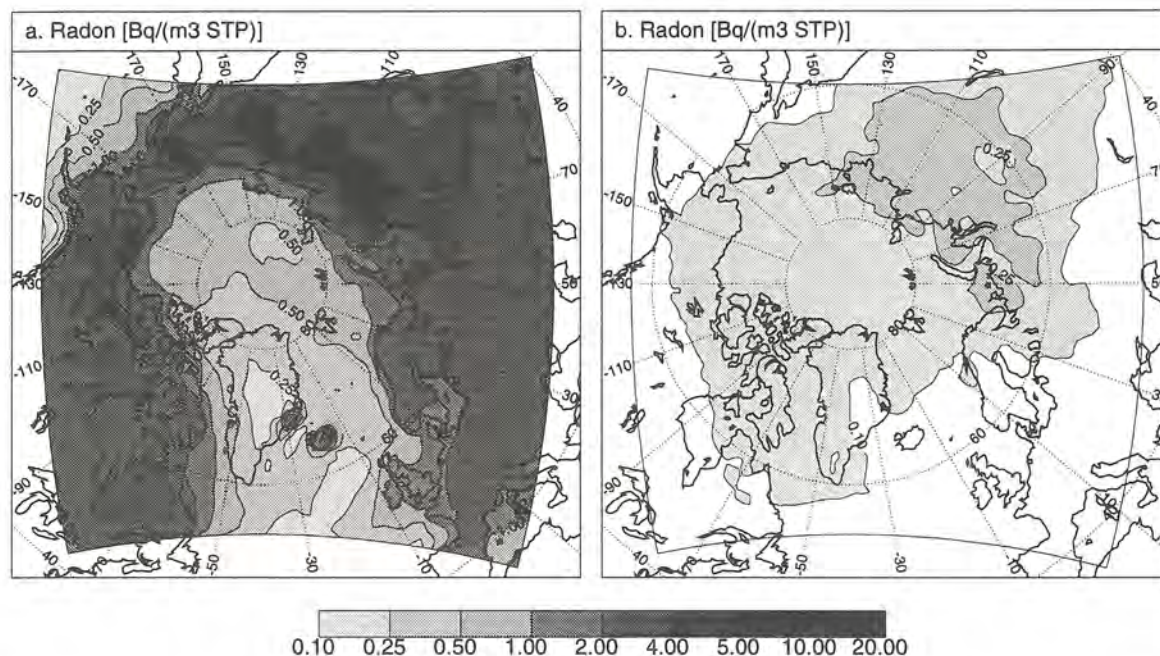


Fig. 12. Mean horizontal distribution of ^{222}Rn for spring and summer and for lowest model layer (left) and layer 15, 6.5 km above ground, (right). Units Bq m^{-3} (STP).

5.6. RESULTS: WINTER

In order to unambiguously distinguish the behavior of our chosen atmospheric boundary layer parameterisations we have deliberately used the same ^{222}Rn flux during winter as during summer. This will probably result in too high ^{222}Rn activity in the model during winter, especially at high latitudes, where the flux to the atmosphere may be inhibited by overlying snow and frozen soil.

Figure 13a shows the temporal evolution of ^{222}Rn activity and boundary layer height over Central Europe (50°N , 10°E) in January and February 1993. In winter, the calculated continental boundary layer is shallow and displays no diurnal variation. The modelled changes in ^{222}Rn activity at this site are primarily due to day-to-day variations in the local boundary layer. ^{222}Rn is generally higher near the surface than in summer and the difference between layer 1 and 5 is also much greater than in summer (cf. Fig. 11a). The same features are even more prominent at the Siberian site (70°N , 110°E), due to a shallower boundary layer.

In locations downwind of the continental source regions (exemplified by the Arctic site in Figure 13c), high ^{222}Rn are occasionally seen as pulses with distinct start- and stop-times. The absolute values and the shape of the peaks are similar to what Worthy *et al.* (1994) reported for Alert (82°N , 62°W) in February ($0.5 - 3 \text{ Bq m}^{-3}$ STP).

Figure 14 shows average ^{222}Rn activity in model-layer 1 (0-60 m) and 15 (ca. 6 km) for February 1994, after the model was allowed to reach a " ^{222}Rn steady state" during January 10-31. Over the emission regions the surface values are typically greater than 5 Bq m^{-3}

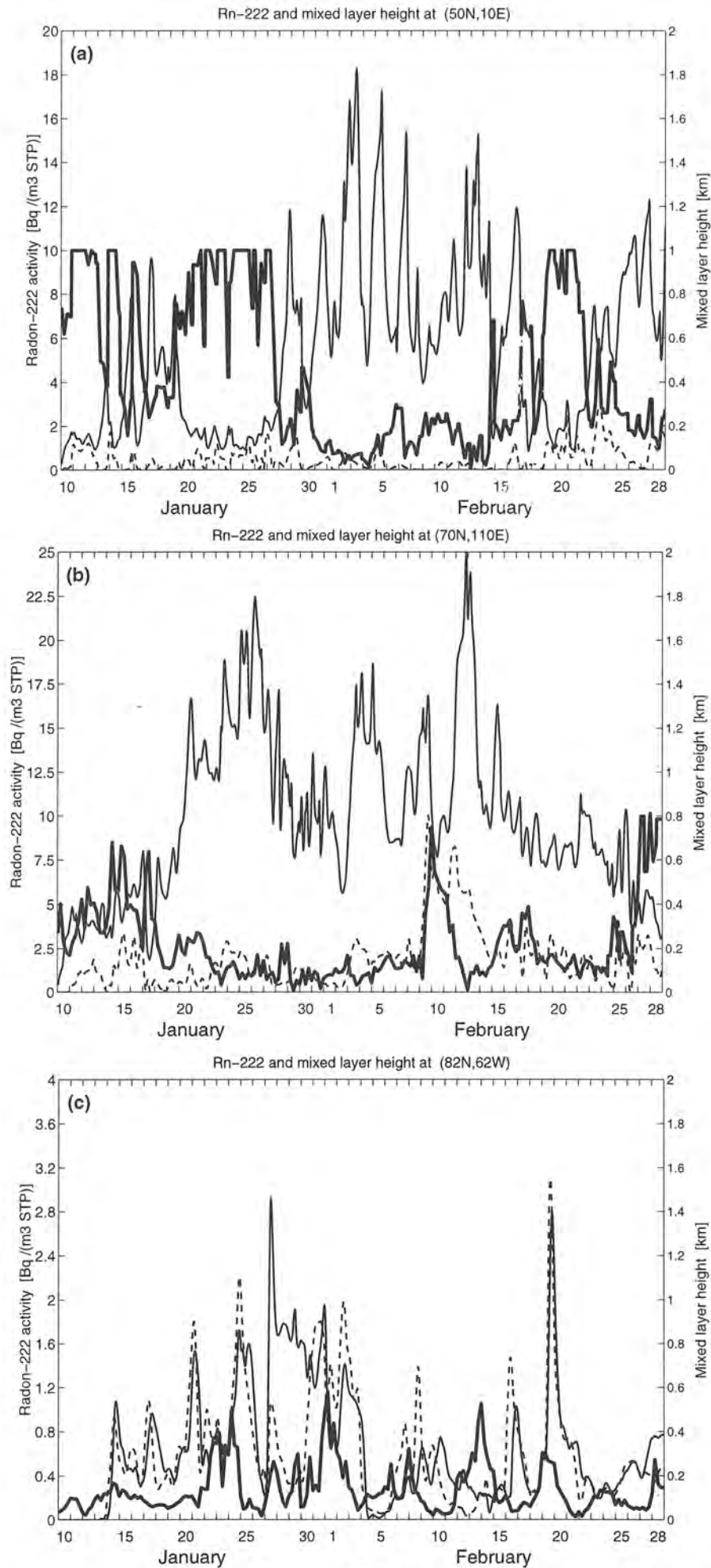


Fig. 13. Calculated boundary layer height, z_{PBL} , and ^{222}Rn activity for a winter period and 3 locations. a) Central Europe (50°N , 10°E), b) Northern Siberia (70°N , 110°E) and c) Canadian Arctic (82°N , 62°W). Thick solid line is boundary layer depth in km; thin solid line is the instantaneous ^{222}Rn activity every 1 hour at the lowest model layer and the dashed line is the corresponding ^{222}Rn activity at model layer 5. Note the different scales in the 3 panels.

(STP), maximum values reach almost 15 Bq m^{-3} (STP). When comparing with summer conditions (Fig. 12) it is obvious that the winter surface ^{222}Rn activity is larger, both over the emission regions and in the ice-covered Arctic. Jacob and Prather (1990) reviewed measurements performed in the USA and showed that the monthly mean concentration near the surface in winter was roughly a factor of 2 greater than in summer (8 and 4

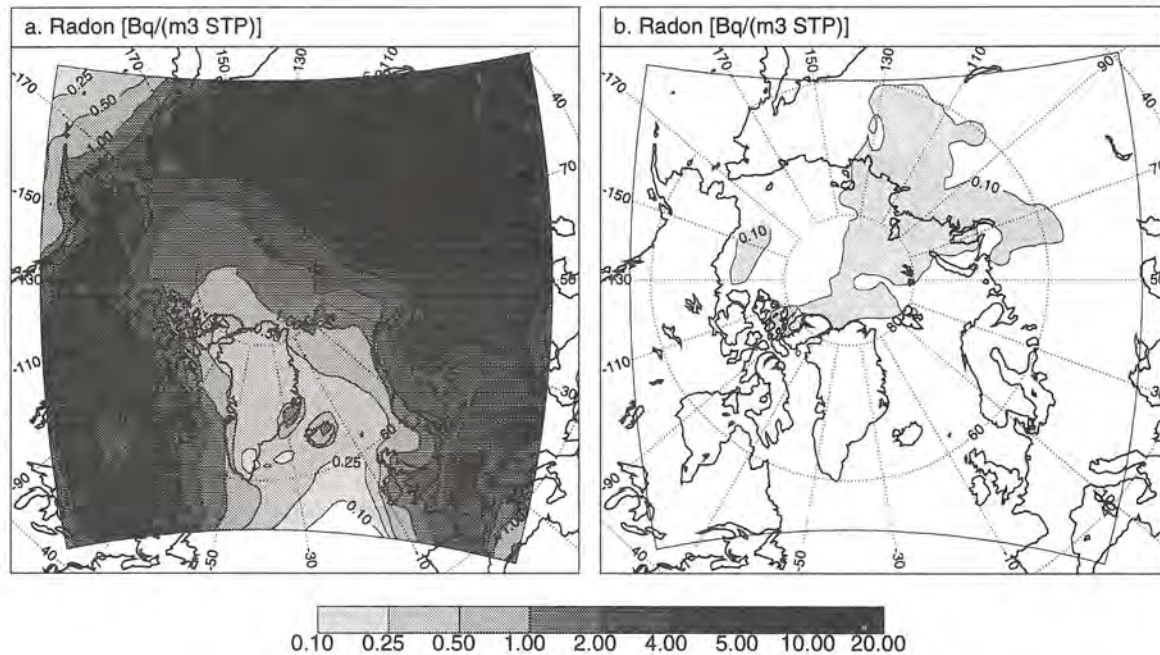


Fig. 14. Mean horizontal distribution of ^{222}Rn for a winter period and for lowest model layer (left) and layer 15, 6.5 km above ground, (right). Units Bq m^{-3} (STP).

Bq m^{-3} (STP) respectively). Similar features were reported for Europe by Feichter and Crutzen (1990), which review data from Freiburg, Germany. The near surface ^{222}Rn in Freiburg had a maxima in November and a minima in March-May (7 and 3 Bq m^{-3} (STP), respectively). At layer 15 the activity is significantly lower during winter than summer which is attributed to the much less efficient vertical mixing then. Maximum average values only barely reaches 0.2 Bq m^{-3} (STP).

A possible problem in these analyses are the assigned zero boundaries. All inflow to the domain will dilute the mixing ratios, this is for example apparent in a wedge over the Atlantic were persistent South-westerly winds brings radon-free air into the domain.

5.7. MEAN VERTICAL DISTRIBUTION

In Figure 15 we display average vertical profiles of ^{222}Rn in MATCH for June 1994 and February 1993. It is clear that the vertical mixing in MATCH is greater in summer than in winter, a feature which is also seen in the measurements of ^{222}Rn displayed in Figures 15a,b. The time-scale for transport from the boundaries to the interior of the domain is less than for transport from the surface to the upper layers of the model. Our profiles and the Liu *et al.* (1984) profiles are therefore strictly not comparable, and the discrepancy will increase the higher up in the domain one gets. Naturally, the difference decreases the farther from the boundaries of MATCH one gets, as indicated in the better correspondence between MATCH and Liu *et al.* (1984) for the Siberian site (Figure 15b) compared to the European site (Figure 15a). It should also be noted that the Liu *et al.* data are a synthesis

of only 23 profiles for summer and 7 for winter the winter profile, and that the uncertainty in the data is considerable, due to the natural variations in ^{222}Rn .

Moore *et al.* (1977) found ^{222}Rn activities of 0.4 Bq m^{-3} (STP) from the surface up to the tropopause in the Eastern Pacific. The lack of negative vertical gradient over oceanic regions, was also confirmed by Andreae *et al.* (1988) who reported constant (ca. 0.2 Bq m^{-3} (STP)), or increasing ^{222}Rn off the coast of Washington, and by Ramonet *et al.* (1996) who often found higher ^{222}Rn at a few km than near the surface of the Atlantic. Wilkniss and Larson (1984) concluded from several years of data in the Arctic that the boundary layer values were typically below 0.5 Bq m^{-3} (STP). Due to a more efficient transport from the source regions in the free troposphere they also often noted similar, or higher, values aloft. As shown in Figure 15c, MATCH simulates similar, constant tropospheric ^{222}Rn , during summer at a remote, Arctic site. During winter, the increased stability over the emission regions is apparent as a monotone decrease of ^{222}Rn above the lowest few layers of the Arctic site.

5.8. COMPARISON WITH OTHER MODELS

Although we have limited measured data for comparison, other model results can be used as additional source of information. Global models typically calculate a slightly higher ^{222}Rn activity near the surface for NH continents during winter than in summer due to less effective mixing wintertime. The few exceptions that appears arise from the formulation of the source function, e.g. suppressed emissions during soil freezing or snow-cover.

Genthon and Armengaud (1995) present near surface, annual mean ^{222}Rn activities over Eurasia and Northern America. The values lie between 2 and 4 Bq m^{-3} (STP). Feichter and Crutzen (1990), Heimann and Feichter (1990), and Balkanski *et al.* (1993) typically allocate the near surface gridsquares of Eurasia ^{222}Rn activities of 2-5 Bq m^{-3} (STP) in summer and 2-10 in winter. The values are slightly lower than ours, which we ascribe to the coarser vertical resolution in these models.

Feichter and Crutzen (1990), and Balkanski *et al.* (1993) simulate ^{222}Rn activity over Eurasia and Northern America at 500 hPa and 6 km respectively to be 0.1-0.2 Bq m^{-3} (STP) in January. Balkanski *et al.* (1993) also give the corresponding values for July which are more than twice as high as their winter values. The mid-tropospheric ^{222}Rn -values of the global models are generally higher than in MATCH (cf. Figures 12b, 14b) which is a consequence of our assigned zero boundaries, which will dilute all ^{222}Rn mixing ratios in the interior of the domain.

5.9. SUMMARY

Using the radioactive tracer ^{222}Rn , we have demonstrated some characteristics of the MATCH transport model.

In section 5.5 and 5.6 we showed that the calculated continental boundary layer undergoes substantial diurnal variation in summer, and that it is generally deeper than in winter. Due to the increased stability in winter, the parameterised vertical mixing in the boundary layer is then smaller and the resulting ^{222}Rn activity close to the ground larger, compared to summer conditions, all in accordance with real data. The near surface ^{222}Rn timeseries and average horizontal distributions for summer, and winter, are very similar to published measurements, both for the continental regions and the more remote, oceanic and Arctic sites.

In section 5.7 we demonstrated that the vertical gradient of ^{222}Rn is very pronounced over a continental site during winter and less so during summer. Over remote regions the ^{222}Rn activity in the model's boundary layer, and the lower troposphere, is rather uniform,

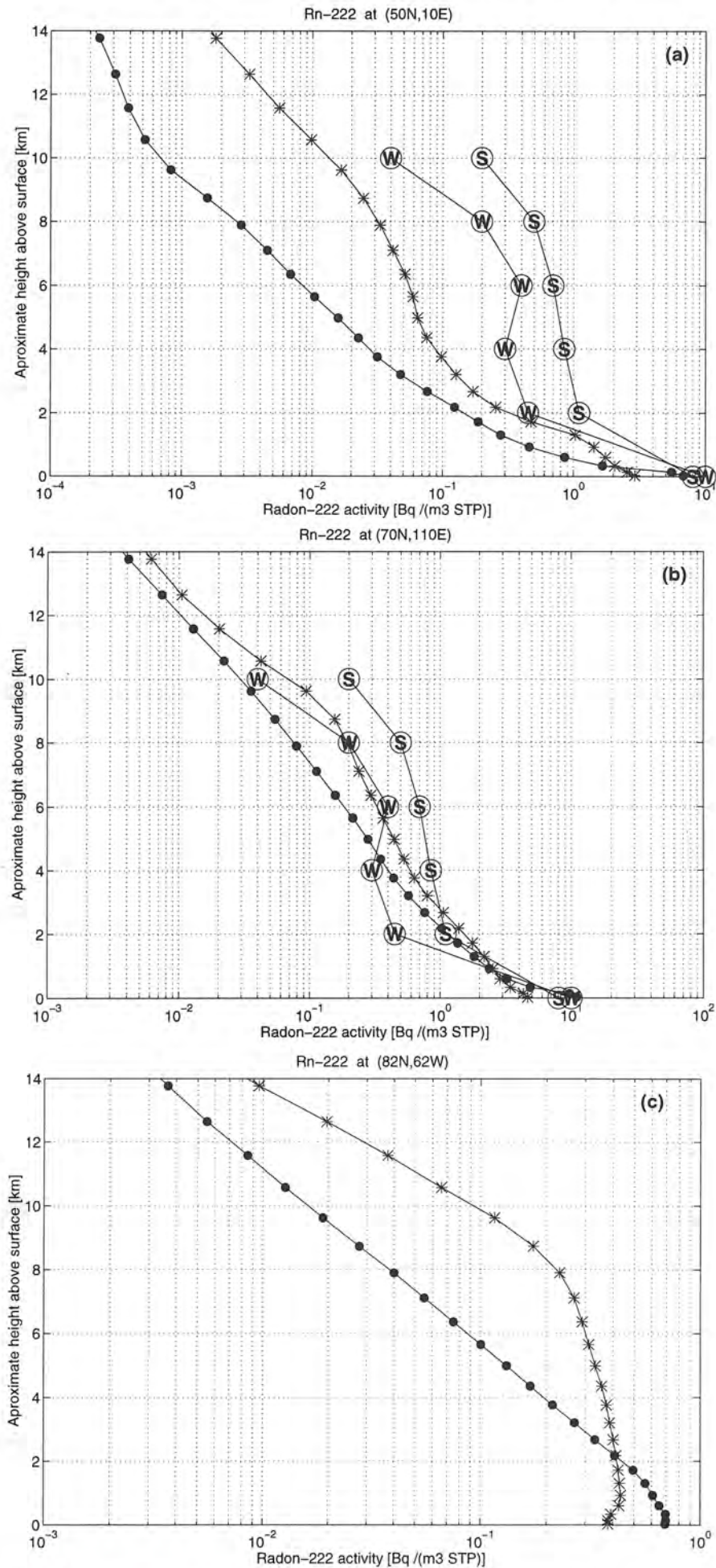


Fig. 15. Simulated mean summer (asterisks), and winter (dots), vertical profiles of ^{222}Rn activity for three locations. a) Central Europe (50°N , 10°E), b) Northern Siberia (70°N , 110°E) and c) Canadian Arctic (82°N , 62°W). In a) and b) are also shown average continental profiles for summer (S) and winter (W) as reviewed by Liu *et al.*, 1984.

especially in summer, features which are all seen in real data. At oceanic and Arctic sites, both the model and real data occasionally show enhanced activity at a few km, due to the more effective horizontal transport there. Moreover, near surface measurements at remote sites often reveal periods with relatively high ^{222}Rn . These episodes are characterized by distinct start and stop times although the emissions occurred several days ago. In section 5.5 and 5.6 we showed that the advection scheme in MATCH was able to maintain sharp gradients in ^{222}Rn mixing ratio with only small diffusion over long periods.

The calculated vertical gradient of ^{222}Rn , discussed in section 5.7 is larger in MATCH than in global transport models and it is probably also to large compared to measurements. This is, however, to be expected since in our experiments the boundaries were assigned zero ^{222}Rn , and the transporttime from the boundaries to a point in the middle of the model-domain is smaller than the transport from the surface up to the middle troposphere. The absence of parameterised deep convection could also contribute discrepancy.

In conclusion, although the available measurements only permits rough comparisons, we have demonstrated reasonable levels of ^{222}Rn activity in MATCH throughout the boundary layer. We have also shown realistic seasonal and spatial variations of ^{222}Rn in the lower troposphere. The only apparent discrepancy between our model and real data can be attributed to the experimental design (i.e. the open boundaries) and the possible impact from deep convection not described, and should be addressed in a forthcoming study.

6. Conclusions

A limited area, off line, Eulerian atmospheric transport model has been developed. The model is designed to be flexible with regard to horizontal and vertical domain and input meteorological data, and provides a framework for application to a wide range of problems in atmospheric transport and chemistry modelling. Mass conservation and maintenance of a positive definite solution is obtained by formulating the equations in flux form. An optional adjustment module which provides a balanced wind field is implemented so that meteorological data from various sources can be utilised. This module makes it possible to also use time interpolated meteorological input data if desired, without loss of accuracy. The test simulations presented clearly demonstrates the ability of the model to meet a number of common requirements on an atmospheric transport model such as mass conservation, positive definiteness, maintenance of constant field and shape preservation. The tests also demonstrates the importance of using balanced wind fields. The simulations of ^{222}Rn indicates qualitatively the ability of the model to simulate a real atmospheric tracer.

Acknowledgements

The MATCH transport model is a result of a continuous development over the last five years. This work was initiated by Christer Persson at SMHI who also was a key person in the development of the first versions of MATCH. His continued support and expertise has been invaluable for the development of the present version. The implementation of η coordinates would not have been possible without the support from the HIRLAM group at SMHI. In particular we have benefited from discussions with Stefan Gollvik and Nils Gustafsson. Special thanks to Elias Hólm for a careful review of the manuscript. We also thank Erland Källén, Hilding Sundqvist and Stephen Craig at the Department of Meteorology, Stockholm University (MISU) for valuable discussions and Henning Rodhe and Kim Holmén for their constructive criticism and continued support. Special thanks go to Ulf Hansson at MISU for guiding one of us (M.E.) through the complicated world of Fortran programs and GRIB-codes.

Appendix

A. Vector increments

Most input parameters read from external sources are normally linearly interpolated in time to yield some higher time resolution. Linear interpolation of wind vectors may, however, cause errors at strong wind shifts, which could be expected predominantly at frontal zones. Vector increments are therefore applied on the wind fields. This is defined by a recursive matrix operation starting with \mathbf{V}^0 which is the wind vector from one set of input data and ending with \mathbf{V}^N from next input of data, and \mathbf{V}^n is all the intermediate (interpolated) wind vectors,

$$\mathbf{V}^{n+1} = A\mathbf{V}^n \quad (\text{A.1})$$

where the matrix A is defined by

$$A = \lambda^{1/N} \begin{pmatrix} \cos(\theta/N) & -\sin(\theta/N) \\ \sin(\theta/N) & \cos(\theta/N) \end{pmatrix} \quad (\text{A.2})$$

where λ and θ are the relative change in wind speed and angular wind shift between two input of data, and N the number of interpolations.

B. Primitive functions

The primitive function of the mass distribution is simply a spatial integral of the mass, defined over a certain interval,

$$Q(x, t) = \int_0^x q(x', t) dx' + C \quad (\text{B.1})$$

where C is an arbitrary constant which we chose to be zero. The interval could be any subdomain of the model area and the coordinate, x , refers to the coordinate within this interval. It is obvious that the primitive function is known exactly at the walls of each grid-cell by summing up the known discrete masses up to each cell wall,

$$Q_i(t) = \sum_{k=0}^i \bar{q}_k(t) \Delta x_k \quad (\text{B.2})$$

where \bar{q} is the discrete value, and k the ‘‘internal’’ index of the grid-cells within the interval selected, and $Q_0 \equiv 0$. This generates set of discrete integral values, Q_0, Q_1, Q_2, \dots , from which a continuous formula can be approximated by some fitting technique. Applying Lagrange polynomial fitting yield,

$$Q(x, t) = \sum_{k=0}^n \alpha_k(x) Q_k(t) \quad (\text{B.3})$$

where the Lagrange polynomial weights are defined by

$$\alpha_k(x) = \prod_{j=0, j \neq k}^n \frac{x - x_j}{x_j - x_k} \quad (\text{B.4})$$

Here x_j represents the coordinates to the cell walls in the local coordinates of the interval, and $x_0 = 0$. Figure 16 shows the relation between a discrete distribution and its

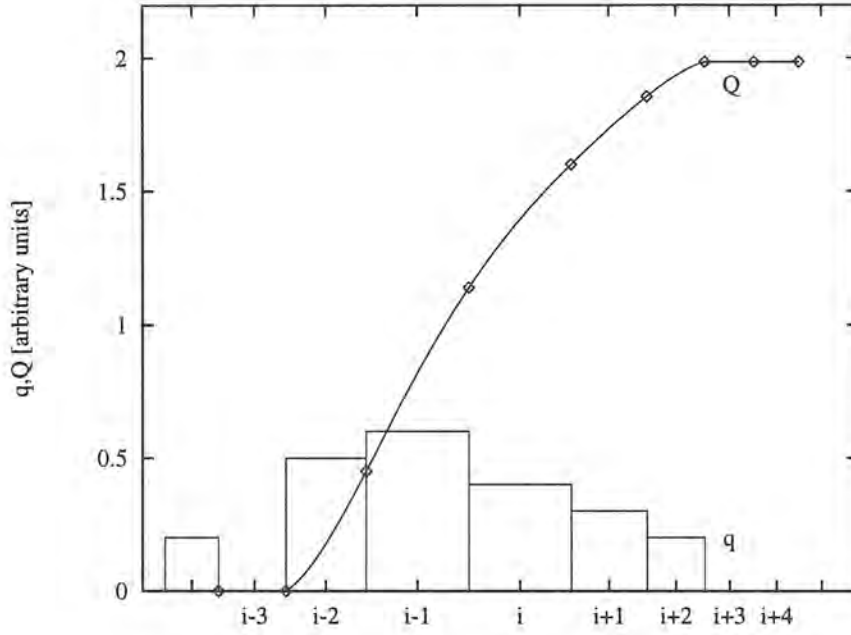


Fig. 16. An example of a discrete distribution and its primitive function defined over the interval $i - 3$ to $i + 4$ (q and Q have different units). The diamonds denote the points where the primitive function is uniquely defined. Note the irregular grid-spacing.

primitive function. The local value and local gradients may be derived by differentiation of the primitive function, thus

$$q(x, t) = \frac{\partial}{\partial x} Q(x, t) = \sum_{k=0}^n \frac{d}{dx} \alpha_k(x) Q_k(t) \quad (\text{B.5})$$

and

$$\frac{\partial}{\partial x} q(x, t) = \frac{\partial^2}{\partial x^2} Q(x, t) = \sum_{k=0}^n \frac{d^2}{dx^2} \alpha_k(x) Q_k(t) \quad (\text{B.6})$$

The momentaneous value could in the same fashion be derived by defining a primitive function in time. Note that the local value at the centre point of a grid-cell may not be equal to the discrete value in this cell.

C. Weights in implicit formulas

The implicit formulation of the vertical diffusion involves the coefficients α and β , referring to the weights of the next and present value, respectively, principally described by

$$q^{t+1} = q^t + \Delta t \left(\alpha \frac{\partial q^{t+1}}{\partial t} + \beta \frac{\partial q^t}{\partial t} \right) \quad (\text{C.1})$$

$$\alpha + \beta = 1 \quad (\text{C.2})$$

The specific choice of values will determine the behavior of the scheme. Selecting $\alpha = 0.0$ and $\beta = 1.0$ leads to an explicit scheme, $\alpha = 0.5$ and $\beta = 0.5$ to a Crank-Nicholson scheme, and $\alpha = 1.5$ and $\beta = -0.5$ to a strongly implicit scheme. We have chosen the

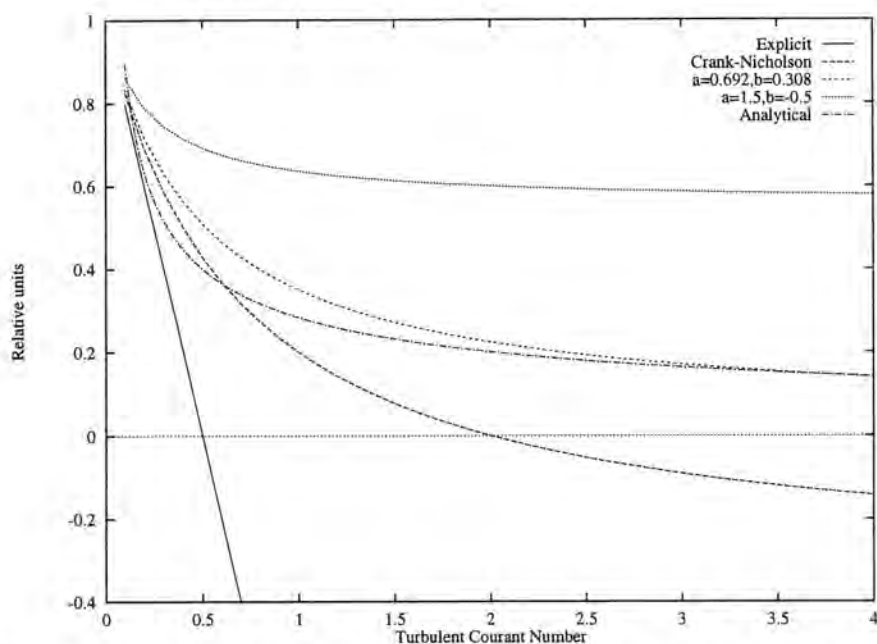


Fig. 17. Diffusion of a peak concentration at various turbulent Courant numbers and for different choices of the implicit formulation.

values $\alpha = 0.692$ and $\beta = 0.308$ justified by the experience that this combination gives the closest agreement to an analytical solution independently of turbulent Courant numbers, as shown in Figure 17. The idealised case refers to a peak concentration diffused by a vertically invariant exchange coefficient.

References

- Andreae, M.O., Berresheim, H., Andreae, T.W., Kritz, M.A., Bates, T.S. and J. T. Merrill, 1988. Vertical distribution of Dimethylsulfide, sulfur dioxide, Aerosol ions, and radon over the Northeast Pacific Ocean. *J. Atmos. Chem.*, **6**, 149-173.
- Balkanski, Y.J., Jacob, D.J., Gardner, G.M., Graustein, W.C., and K. K. Turekian, 1993. Transport and residence times of tropospheric aerosols inferred from a global three-dimensional simulation of ^{210}Pb . *J. Geophys. Res.*, **D98**, 20573-20586.
- Berkowicz, R., Olesen, H.R. and U. Torp, 1986. The danish Gaussian air pollution model (OML): Description, test and sensitivity analysis in view of regulatory applications. *Proceedings of the Fifteenth NATO/CCMS International Technical Meeting on Air Pollution Modeling and Its Application*, April 15-19, St. Louis, Missouri, 453-481.
- Bott, A., 1989a. A positive definite advection scheme obtained by nonlinear renormalization of advective fluxes. *Monthly Weather Rev.*, **117**, 1006-1015.
- Bott, A., 1989b. Reply. Notes and correspondance. *Monthly Weather Rev.*, **117**, 2633-2636.
- Bott, A., 1992. Monotone flux limitaion in the area-preserving flux-form advection algorithm. *Monthly Weather Rev.*, **120**, 2592-2602.
- Broecker, W.S., Li, Y.H. and J. Cromwell, 1967. Radium-226 and radon-222 concentration in Atlantic and Pacific oceans. *Science*, **158**, 1307-1310.
- Burridge, D. M. and A. J. Gadd, 1977. The meteorological office operational 10-level numerical Weather prediction model. *Sc. Paper*, No **34**, Meteor. Office, London Road, Bracknell, Berkshire RG12 2sz, England, 1-39.
- Businger, J.A., Wyngaard, J.C., Izumi, Y., and E.F. Bradley, 1971. Flux profile relationships in the atmospheric surface layer. *J. Atmos. Sci.*, **28**, 181-189.
- Carmichel, G. R. and L. K. Peters, 1984. An Eulerian transport/transformation/removal model for SO_2 and sulfate-I. Model development. *Atmos. Environ.*, **18**, 937-951.
- Cats, G.J, de Haan, B.J. and L.M. Hafkenschied. Verification of an objective analysis scheme. Meteorological analyses after the Chernobyl disaster verified by trajectories of radioactive air masses. *KNMI scientific report WR 87-4*.

- Chang, J. S., Brost, R. A., Isaksen, I. S. A., Madronich, S., Middleton, P., Stockwell, W. R. and C. J. Walcek, 1987. A three-dimensional Eulerian acid deposition model. Physical concept and model formulation. *J. Geophys. Res.*, **92**, 14681-14700.
- Crowley, W. P., 1968. Numerical advection experiments. *Monthly Weather Rev.*, **96**, 1-11.
- Dardub, D. and J. H. Seinfeld, 1994. Numerical advective schemes used in air quality models. Sequential and parallel implementation. *Atmos. Environ.*, **28**, No 20, 3369-3385.
- Dörr, H., Kromer, B., Levin, I., München, K.O. and H.-J. Volpp, 1983. CO₂ and Radon 222 as tracers for atmospheric transport. *J. Geophys. Res.*, **C88**, 1309-1313.
- Ebel, A., Hass, H., Jacobs, H. J., Memmersheimer M., Laube, M. and A. Oberreuter, 1991. Simulation of ozone intrusion caused by a tropopause fold and cut-off low. *Atmos. Environ.*, **24**, 2131-2144.
- Feichter, J. and P.J. Crutzen, 1990. Parameterization of vertical tracer transport due to deep cumulus convection in a global transport model and its evaluation with ²²²Rn measurements. *Tellus*, **42B**, 100-117.
- Feichter, J., Brost, R.A. and M. Heimann, 1991. Three-dimensional modeling of the concentration and deposition of ²¹⁰Pb aerosols. *J. Geophys. Res.*, **D96**, 22447-22460.
- Genthon, C. and A. Armengaud, 1995. Radon 222 as a comparative tracer of transport and mixing in two general circulation models of the atmosphere. *J. Geophys. Res.*, **D100**, 2849-2866.
- Graustein, W.C. and K.K. Turekian, 1990. Radon fluxes from soils to the atmosphere measured by ²¹⁰Pb - ²²⁶Ra disequilibrium in soils. *Geophys. Res. Lett.*, **17**, 841-844.
- Grasty, R.L. 1992. Summer outdoor radon variations in Canada and their relation to soil moisture. *Health Physics*, **66**, 185-193.
- Heimann, M. and J. Feichter, 1990. A comparison of three-dimensional atmospheric transport models by means of simulations of Radon-222. *Rep. 8*, Meteorol. Inst., Univ. Hamburg, Germany.
- Heimann, M. and C.D. Keeling, 1989. A three-dimensional model of atmospheric CO₂ transport based on observed winds. 2. Model description and simulated tracer experiments. In: *Aspects of Climate Variability in the Pacific and the Western Americas* (ed. D.H. Peterson). American Geophysical Union, Washington, DC, pp 237-275.
- Hólm, E. V., 1994. A fully two-dimensional non-oscillatory advection scheme for momentum and scalar transport equations. *Monthly Weather Rev.*, **123**, 536-552.
- Holtstag, A. A. M., Meijgaard, E. van and W. C. De Rooy, 1995. A comparison of boundary layer diffusion schemes in unstable conditions over land. *Boundary-Layer Met.*, **76**, 69-95.
- Jacob, D.J. and M.J. Prather, 1990. Radon-222 as a test of convective transport in a general circulation model. *Tellus*, **42B**, 118-134.
- Källén, E., 1996. *HIRLAM documentation manual - System 2.5*. Norrköping, June 1996.
- Lambert, G., Polian, G., Sanak, J., Ardouin, B., Buisson, A., Jegou, A. and J.C. Le Rouley, 1982. Radon and daughter products cycle. Application to troposphere-stratosphere exchanges (in French). *Ann Géophys.*, **38**, 4, 497-531.
- Langner, J., Persson, C., Robertson, L. and A. Ullerstig, 1996. Air pollution assessment study using the MATCH modelling system. Application to sulfur and nitrogen compounds over Sweden 1994. *Swedish Meteorological and Hydrological Institute, RMK-69*.
- Langner, J., Persson, C. and L. Robertsson, 1995. Concentration and deposition of acidifying air pollutants over Sweden. Estimates for 1991 based on the MATCH model and observations. *Water Air and Soil Poll.*, **85**, 2021-2026.
- Langner, J. and H. Rodhe, 1991. A global three-dimensional model of the troposphere sulfur cycle. *J. Atmos. Chem.*, **13**, 225-263.
- Larson, R.E., 1974. Radon profiles over Kilauea, the Hawaiian Islands and Yukon Valley snow cover. *Pure Appl. Geophys.*, **112**, 204-208.
- Larson, R.E., Lamontagne, R.A. and P.E. Wilkniss, 1972. Radon-222, CO, CH₄ and continental dust over the Greenland and Norwegian seas. *Nature* **240**, 345-347.
- Leck, C. Bigg, E.K., Covert, D.S., Heintzenberg, J., Maenhaut, W., Nilsson, E.D. and A. Wiedensohler, 1996. Overview of the atmospheric research program during the International Arctic Ocean Expedition of 1991 (IAOE-91) and its scientific results. *Tellus*, **48B**, 136-155.
- Leslie, L. M. and R. J. Purser, 1995. Three-dimensional mass-conservative semi-Lagrangian scheme employing forward trajectories. *Monthly Weather Rev.*, **123**, 2551-2566.
- Liu, S.C. McAfee, J.R. and R.J. Cicerone, 1984. Radon-222 and tropospheric vertical transport. *J. Geophys. Res.*, **D89**, 7291-7297.
- Mattson, R., 1970. Seasonal variation of short-lived radon progeny, ²¹⁰Pb and ²¹⁰Po, in ground level air in Finland. *J. Geophys. Res.*, **75**, 1741-1744.
- Maenhaut, W., Zoller, W.H. and D.G. Coles, 1979. Radio nuclides in the South Pole atmosphere. *J. Geophys. Res.*, **84**, 3131-3138.
- Moore, H.E., Poet, S.E. and E.A. Martell, 1977. Vertical profiles of ²²²Rn and its long-lived daughters over the Eastern Pacific. *Environ. Sci. Technol.*, **11** 1207-1210.
- Ostiguy, L. and J. P. R. Laprise, 1990. On the positivity of mass in common used numerical transport schemes. *Atmosphere-Ocean*, **28** (2), 147-161.

- Persson, C., Robertson, L., Häggkvist, K. and L. Meuller, 1990. Mesoskalig spridningsmodell - Modelanpassning till Skånergionen, *Swedish Meteorological and Hydrological Institute, Rapport-Meteorologi*, (partly in Swedish).
- Persson, C., Langner, J. and L. Robertson, 1994. A mesoscale air pollution dispersion model for the Swedish west-coast region - Air pollution assessment for the year 1991. *Swedish Meteorological and Hydrological Institute, RMK-65*.
- Polian, G. Lambert, G. Ardouin, B. and A. Jegou, 1986. Long-range transport of continental radon in subantarctic and antarctic areas. *Tellus*, **38B**, 178-189.
- Ramonet, M., Roulley, le J.C., Bousquet, P. and P. Monfray, 1996. Radon-222 measurements during the Tropoz II campaign and comparison with a global atmospheric model. *J. Atmos. Chem.*, **23**, 107-136.
- Rash, P.J. and D.L. Williamson, 1990. Computational aspects of moisture transport in global models of the atmosphere. *Quart. J. Roy. Meteor. Soc.*, **116** Part B, 1071-1090.
- Rash, P. J., 1993. Conservative shape-preserving two-dimensional transport on a spherical reduced grid. *Monthly Weather Rev.*, **122**, 1337-1350.
- Ritchie, H., 1985. elimination of the interpolation associated with semi-Lagrangian Schemes. *Monthly Weather Rev.*, **114**, No. 1, 135-146.
- Schery, S.D., Gaeddert, D.H. and M.H. Wilkening, 1984. Factors affecting exhalation of radon from a gravelly sandy loam. *J. Geophys. Res.*, **89**, 7299-7309.
- Schery, S.D, Whittlestone, S., Hart, K.P. and S.E. Hill, 1989. The flux of radon and thoron from Australian soils. *J. Geophys. Res.*, **D94**, 8567-8576.
- Tremback, C. J., Powel, J., Cotton, W. R. and R. A. Pielke, 1987. The forward-in-time advection transport algorithm. Extensions to higher orders. *Monthly Weather Rev.*, **115**, 540-555.
- Turekian, K.K., Nozaki, Y. and L.K. Benninger, 1977. Geochemistry of atmospheric radon and radon products. *Ann. Rev. Earth Planet. Sci.*, **5**, 227-255.
- van Ulden, A.P. and A.A.M. Holtslag, 1985. Estimation of atmospheric boundary layer parameters for diffusion applications. *J. Climate Appl. Met.*, **24**, 1196-1207.
- Wilkening, M.H. and Clements, W.E., 1975. Radon 222 from the ocean surface. *J. Geophys. Res.*, **80**, 3828-3830.
- Wilkening, M.H., Clements, W.E. and D. Stanley, 1972. Radon-222 flux measurements in widely separated regions. In: *The Natural Radiation Environment, Vol II*, 717-730. National Technical Information Service, Springfield, Va.
- Wilkniess, P.E. and R.E. Larson, 1984. Atmospheric radon measurements in the Arctic; fronts, seasonal observations, and transport of continental air to polar regions. *J. Atmos. Sci.*, **41**, 2347-2358.
- Williamson, D. L., 1989. Semi-Lagrangian moisture transport in the NMC spectral model. *Tellus*, **42A**, No. 4, 413-420.
- Williamson, D. L., and P. J. Rash, 1988. Two-dimensional semi-Lagrangian transport with shape-preserving interpolation. *Monthly Weather Rev.*, **117**, No. 1, 102-129.
- Worthy, D.E.J., Trivett, N.B.A., Hopper, J.F., Bottenheim, J.W. and I. Levin, 1994. Analysis of long-range transport events at Alert, Northwest territories, during the polar sunrise experiment. *J. Geophys. Res.*, **D99**, 25329-25344.
- Zilitinkevich, S. and D.V. Moronov, 1996. A multi-limit formulation for the equilibrium depth of a stably stratified boundary layer. *Max-Planck-Institut for Meteorology, Report No. 185*, ISSN 0397-1060, 30 pp. (To appear in *Boundary-Layer Meteorol.*)

SMHIs publications

SMHI publishes six report series. Three of these, the R-series, are intended for international readers and are in most cases written in English. For the others the Swedish language is used.

Names of the Series	Published since
RMK (Report Meteorology och Climatology)	1974
RH (Report Hydrology)	1990
RO (Report Oceanography)	1986
METEOROLOGI	1985
HYDROLOGI	1985
OCEANOGRAFI	1985

Earlier issues published in serie RMK

- 1 Thompson, T., Udin, I., and Omstedt, A. (1974)
Sea surface temperatures in waters surrounding Sweden.
- 2 Bodin, S. (1974)
Development on an unsteady atmospheric boundary layer model.
- 3 Moen, L. (1975)
A multi-level quasi-geostrophic model for short range weather predictions.
- 4 Holmström, I. (1976)
Optimization of atmospheric models.
- 5 Collins, W.G. (1976)
A parameterization model for calculation of vertical fluxes of momentum due to terrain induced gravity waves.
- 6 Nyberg, A. (1976)
On transport of sulphur over the North Atlantic.
- 7 Lundqvist, J.-E., and Udin, I. (1977)
Ice accretion on ships with special emphasis on Baltic conditions.
- 8 Eriksson, B. (1977)
Den dagliga och årliga variationen av temperatur, fuktighet och vindhastighet vid några orter i Sverige.
- 9 Holmström, I., and Stokes, J. (1978)
Statistical forecasting of sea level changes in the Baltic.
- 10 Omstedt, A., and Sahlberg, J. (1978)
Some results from a joint Swedish-Finnish sea ice experiment, March, 1977.
- 11 Haag, T. (1978)
Byggnadsindustrins väderberoende, seminarieuppsats i företagsekonomi, B-nivå.
- 12 Eriksson, B. (1978)
Vegetationsperioden i Sverige beräknad från temperaturobservationer.
- 13 Bodin, S. (1979)
En numerisk prognosmodell för det atmosfäriska gränsskiktet, grundad på den turbulenta energiekvationen.
- 14 Eriksson, B. (1979)
Temperaturfluktuationer under senaste 100 åren.
- 15 Udin, I., och Mattisson, I. (1979)
Havsis- och snöinformation ur datorbearbetade satellitdata - en modellstudie.
- 16 Eriksson, B. (1979)
Statistisk analys av nederbördsdata. Del I. Arealnederbörd.
- 17 Eriksson, B. (1980)
Statistisk analys av nederbördsdata. Del II. Frekvensanalys av månadsnederbörd.

- 18 Eriksson, B. (1980)
Årsmedelvärdet (1931-60) av nederbörd, avdunstning och avrinning.
- 19 Omstedt, A. (1980)
A sensitivity analysis of steady, free floating ice.
- 20 Persson, C., och Omstedt, G. (1980)
En modell för beräkning av luftföroreningars spridning och deposition på mesoskala.
- 21 Jansson, D. (1980)
Studier av temperaturinversioner och vertikal vindskjuvning vid Sundsvall-Härnösands flygplats.
- 22 Sahlberg, J., and Törnevik, H. (1980)
A study of large scale cooling in the Bay of Bothnia.
- 23 Ericson, K., and Hårsmar, P.-O. (1980)
Boundary layer measurements at Klockrike. Oct. 1977.
- 24 Bringfelt, B. (1980)
A comparison of forest evapotranspiration determined by some independent methods.
- 25 Bodin, S., and Fredriksson, U. (1980)
Uncertainty in wind forecasting for wind power networks.
- 26 Eriksson, B. (1980)
Graddagsstatistik för Sverige.
- 27 Eriksson, B. (1981)
Statistisk analys av nederbördsdata. Del III. 200-åriga nederbördsserier.
- 28 Eriksson, B. (1981)
Den "potentiella" evapotranspirationen i Sverige.
- 29 Pershagen, H. (1981)
Maximisnödjun i Sverige (perioden 1905-70).
- 30 Lönnqvist, O. (1981)
Nederbördsstatistik med praktiska tillämpningar. (Precipitation statistics with practical applications.)
- 31 Melgarejo, J.W. (1981)
Similarity theory and resistance laws for the atmospheric boundary layer.
- 32 Liljas, E. (1981)
Analys av moln och nederbörd genom automatisk klassning av AVHRR-data.
- 33 Ericson, K. (1982)
Atmospheric boundary layer field experiment in Sweden 1980, GOTEX II, part I.
- 34 Schoeffler, P. (1982)
Dissipation, dispersion and stability of numerical schemes for advection and diffusion.
- 35 Undén, P. (1982)
The Swedish Limited Area Model. Part A. Formulation.
- 36 Bringfelt, B. (1982)
A forest evapotranspiration model using synoptic data.
- 37 Omstedt, G. (1982)
Spridning av luftförorening från skorsten i konvektiva gränsskikt.
- 38 Törnevik, H. (1982)
An aerobiological model for operational forecasts of pollen concentration in the air.
- 39 Eriksson, B. (1982)
Data rörande Sveriges temperaturklimat.
- 40 Omstedt, G. (1984)
An operational air pollution model using routine meteorological data.
- 41 Persson, C., and Funkquist, L. (1984)
Local scale plume model for nitrogen oxides. Model description.
- 42 Gollvik, S. (1984)
Estimation of orographic precipitation by dynamical interpretation of synoptic model data.
- 43 Lönnqvist, O. (1984)
Congression - A fast regression technique with a great number of functions of all predictors.
- 44 Laurin, S. (1984)
Population exposure to SO_2 and NO_x from different sources in Stockholm.
- 45 Svensson, J. (1985)
Remote sensing of atmospheric temperature profiles by TIROS Operational Vertical Sounder.

- 46 Eriksson, B. (1986)
Nederbörds- och humiditetsklimat i Sverige under vegetationsperioden.
- 47 Taesler, R. (1986)
Köldperioden av olika längd och förekomst.
- 48 Wu Zengmao (1986)
Numerical study of lake-land breeze over Lake Vättern, Sweden.
- 49 Wu Zengmao (1986)
Numerical analysis of initialization procedure in a two-dimensional lake breeze model.
- 50 Persson, C. (1986)
Local scale plume model for nitrogen oxides. Verification.
- 51 Melgarejo, J.W. (1986)
An analytical model of the boundary layer above sloping terrain with an application to observations in Antarctica.
- 52 Bringfelt, B. (1986)
Test of a forest evapotranspiration model.
- 53 Josefsson, W. (1986)
Solar ultraviolet radiation in Sweden.
- 54 Dahlström, B. (1986)
Determination of areal precipitation for the Baltic Sea.
- 55 Persson, C. (SMHI), Rodhe, H. (MISU), De Geer, L.-E. (FOA) (1986)
The Chernobyl accident - A meteorological analysis of how radionuclides reached Sweden.
- 56 Persson, C., Robertsson, L. (SMHI), Grennfelt, P., Kindbom, K., Lövblad, G., och Svanberg, P.-A. (IVL) (1987)
Luftföroreningsepisoden över södra Sverige 2 - 4 februari 1987.
- 57 Omstedt, G. (1988)
An operational air pollution model.
- 58 Alexandersson, H., Eriksson, B. (1989)
Climate fluctuations in Sweden 1860 - 1987.
- 59 Eriksson, B. (1989)
Snödjupsförhållanden i Sverige - Säsongerna 1950/51 - 1979/80.
- 60 Omstedt, G., Szegö, J. (1990)
Människors exponering för luftföroreningar.
- 61 Mueller, L., Robertson, L., Andersson, E., Gustafsson, N. (1990)
Meso- γ scale objective analysis of near surface temperature, humidity and wind, and its application in air pollution modeling.
- 62 Andersson, T., Mattisson, I. (1991)
A field test of thermometer screens.
- 63 Alexandersson, H., Gollvik, S., Mueller, L. (1991)
An energy balance model for prediction of surface temperatures.
- 64 Alexandersson, H., Dahlström, B. (1992)
Future climate in the Nordic region - survey and synthesis for the next century.
- 65 Persson, C., Langner, J., Robertson, L. (1994)
Regional spridningsmodell för Göteborgs och Bohus, Hallands och Älvsborgs län. (A mesoscale air pollution dispersion model for the Swedish west-coast region. In Swedish with captions also in English.)
- 66 Karlsson, K.-G. (1994)
Satellite-estimated cloudiness from NOAA AVHRR data in the Nordic area during 1993.
- 67 Karlsson, K.-G. (1996)
Cloud classifications with the SCANDIA model.
- 68 Persson, C., Ullerstig, A. (1996)
Model calculations of dispersion of lindane over Europe. Pilot study with comparisons to measurements around the Baltic Sea and the Kattegat.
- 69 Langner, J., Persson, C., Robertson, L., and Ullerstig, A. (1996)
Air pollution Assessment Study Using the MATCH Modelling System. Application to sulfur and nitrogen compounds over Sweden 1994.



Swedish Meteorological and Hydrological Institute
S-601 76 Norrköping, Sweden. Tel. +4611158000. Telex 644 00 smhi s.

ISSN 0347-2116